Icarus 386 (2022) 115169

Contents lists available at ScienceDirect

Icarus

journal homepage: www.elsevier.com/locate/icarus

Convective storms in closed cyclones in Jupiter: (II) numerical modeling

Peio Iñurrigarro [a,*], Ricardo Hueso [a], Agustín Sánchez-Lavega [a], Jon Legarreta [b]

[a] Física Aplicada, Escuela de Ingeniería de Bilbao, Universidad del País Vasco UPV/EHU, Plaza Ingeniero Torres Quevedo, 1, 48013 Bilbao, Spain
[b] Ingeniería de Sistemas y Automática, Escuela de Ingeniería de Bilbao, Universidad del País Vasco UPV/EHU, Plaza Ingeniero Torres Quevedo, 1, 48013 Bilbao, Spain

ARTICLE INFO

Keywords:
Jupiter
Atmosphere
Dynamics

ABSTRACT

On May 31, 2020 a convective storm appeared in one small cyclone in the South Temperate Belt (STB) of Jupiter. The storm, nicknamed as Clyde's Spot, had an explosive start and quickly diminished in activity in a few days. However, it left a highly turbulent cyclone as a remnant that evolved to become a turbulent segment of the STB in a time-scale of one year. A very similar storm erupted on August 7, 2021 in another cyclone of the STB with a similar initial phenomenology. In both cases, the outbreaks started in cyclones that were the result of the merger of pre-existing vortices. In a previous paper we presented an observational study of these storms compared with a similar cyclonic convective system observed during the Voyager 2 flyby [*Hueso* et al., *Convective storms in closed cyclones in Jupiter's South Temperate Belt: (I) Observations, Icarus, 380, 2022*]. Here we present numerical simulations of these vortices and storms with the Explicit Planetary Isentropic-Coordinate (EPIC) numerical model. We simulate mergers of cyclones in Jupiter's STB and investigate the deep structure of the resulting cyclone and its capability to uplift material from the water condensation level. Convection is introduced in the model imposing heating sources whose vertical extent, horizontal size and duration are free parameters that we explore. Our simulations reproduce the cloud field of both storms after short episodes of a few hours of intense convection. The evolution of the morphology of the convective cyclone after the convective pulse stopped shows a strong relation between the convective energy released and the initial vorticity in the cyclone. Similar results are obtained for the cyclonic storm observed during the Voyager 2 flyby. We also compare our simulations of these storms with numerical simulations of a storm that developed in the STB in 2018 inside an elongated cyclone known as the South Temperate Belt Ghost [*Iñurrigarro* et al., *Observations and numerical modelling of a convective disturbance in a large-scale cyclone in Jupiter's South Temperate Belt, Icarus, 336, 2020*]. In addition, we also simulate one of the large-scale storms that develop in the South Equatorial Belt comparing our simulations with Voyager 1 observations of one of those events. From these simulations, we establish a relative scale of energies associated to these convective storms. As coherent cyclones isolate the local atmosphere from their surroundings, we propose that the availability of condensables inside closed cyclones limits the duration of active convection, allowing larger convective outbursts in larger cyclones. Our simulations of the short and intense convective pulse associated to the 2020 and 2021 STB suggest a minimum local water abundance of 1.0–1.2 times solar at the location of the storms. The lower number considers a significant contribution of ammonia condensation, and the larger number considers only water moist convection with a negligible role of ammonia.

1. Introduction

Moist convection is driven by the release of latent heat. In Jupiter's atmosphere this is a process of paramount importance that occurs predominantly in regions of cyclonic shear and under a variety of spatial scales (Ingersoll et al., 2004; Vasavada and Showman, 2005). Observationally, large convective storms can transform the visual aspect of specific bands (Sánchez-Lavega and Gómez, 1996; Sánchez-Lavega et al., 2008, 2017; Fletcher et al., 2017), and strong but short-lived convective events can modify entire segments of a band (Iñurrigarro et al., 2020; Hueso et al., 2022). Convective storms are proposed to be a major contribution of energy to the zonal jets through the creation of eddies that interact with the jets (Ingersoll et al., 2000; Vasavada and Showman, 2005; Lian and Showman, 2010) following an inverse cascade of energy (Young and Read, 2017). However, there is some dispute in the origin of the eddies, as both moist convection and

* Corresponding author.
E-mail address: peio.inurrigarro@ehu.eus (P. Iñurrigarro).

https://doi.org/10.1016/j.icarus.2022.115169
Received 22 April 2022; Received in revised form 9 June 2022; Accepted 29 June 2022
Available online 5 July 2022

baroclinic instabilities seem possible drivers of this activity (Read et al., 2020).

In Jupiter, ammonia and water can produce moist convective storms, but water condensation releases more energy because of its larger latent heat and its expected higher molecular abundance well below the observable clouds. Lightning observations at depths of $\geq$3 bar (Little et al., 1999; Gierasch et al., 2000) link moist convective storms to water condensation. Lightning activity occurs with different frequency on different latitudes and during the early Juno mission (2016–2017) it was observed to be higher in the polar regions, absent in the equator and very infrequent in the South Temperate Belt (Brown et al., 2018). In addition, water moist convection has been proposed to explain the global desiccation of tropospheric ammonia below the upper clouds observed by Juno at all latitudes except the equator (Li et al., 2017). The proposed mechanism is that vertically extended storms can lead to the formation and precipitation of large water-ammonia "mushballs" that fall down to deep layers desiccating the upper atmosphere (Guillot et al., 2020a, 2020b). The global effects of convection contrast with observations of storms at the clouds, where storms powerful enough to produce intense convection with high clouds and intense dynamics occur rarely, with very strong outbursts occurring cyclically in some latitudes (Fletcher, 2017).

Comparisons of moist convective models with observations of Jovian storms should help to understand the processes outlined above. However, the time and spatial scales in which convective storms operate, and the limitations of the observations, generally constrained to the upper cloud level, make those comparisons challenging. Some existing comparisons relay on the altitude of cloud tops and the predictions from convective models (i.e. Stoker, 1986; Hueso and Sánchez-Lavega, 2001; Sánchez-Lavega et al., 2008). Other authors examine simulations that reproduce the cloud morphologies observed in specific convective storms (Hueso et al., 2002; García-Melendo et al., 2005; Sánchez-Lavega et al., 2008; Iñurrigarro et al., 2020). Additional models focus on studying the global effects of moist convection on the vertical structure of the atmosphere (Sugiyama et al., 2014), or in the evaluation of the overall frequency of convective activity at different latitudes (Sankar and Palotai, 2022).

Recently, a short-lived mid-size storm (~4600 km at its peak) erupting at planetographic latitude −30.8° in the South Temperate Belt (STB), was observed in exquisite detail along its life-cycle (Hueso et al., 2022). The storm started on May 31, 2020 as a bright and compact cloud in methane band images erupting in the center of a pre-existing cyclone and was known as "Clyde's Spot" after the name of the observer who obtained the first image of the storm (Foster et al., 2020). A combination of amateur, Hubble Space Telescope (HST) and Junocam images showed how the initial compact cyclone (Fig. 1a) transformed into a double-lobed storm system in 2–3 days (Fig. 1b). On August 7, 2021 a new storm developed in a similar cyclone in the STB, and its early stages were observed by several amateur astronomers with images that also showed the double-lobed shape (Fig. 1c). After a very similar start and early

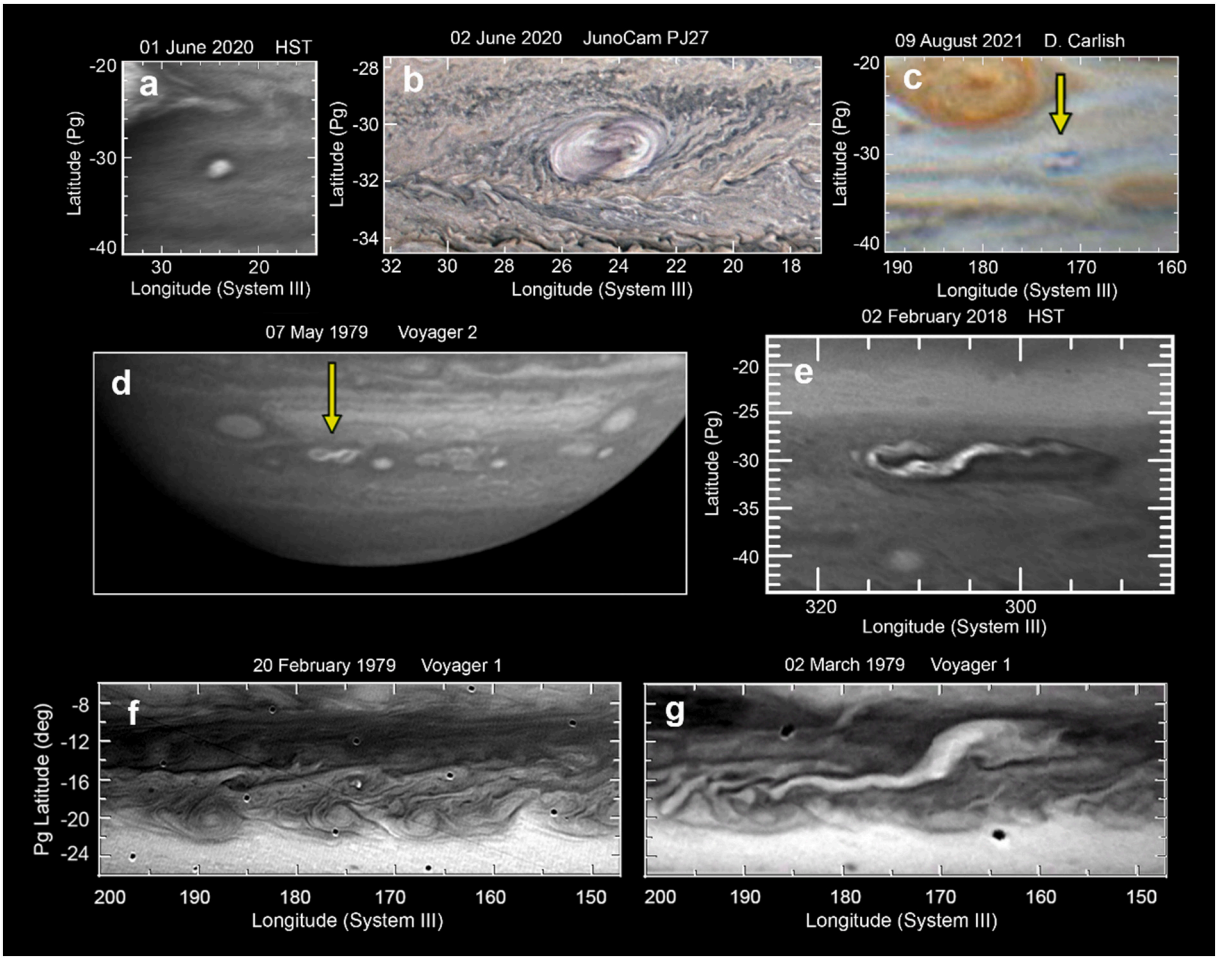

Fig. 1. Summary of the features discussed in this paper. (a) Clyde's Spot as observed at the methane-absorption band by HST 2 days after its onset, and (b) by Junocam on visible light an additional Jupiter rotation later. (c) The August 2021 convective storm in an amateur observation obtained 2 days after the convective eruption. (d) Voyager 2 image of Jupiter showing the development of a convective perturbation at planetographic latitude 38.8°S in a cyclone also imaged 2 days after the start of the convective outburst. (e) The storm in the STB Ghost observed in methane-band 3 days after the start of convection (Iñurrigarro et al., 2020). (f) and (g) two of the images of the SEB storm discussed in Hueso et al. (2002) and imaged one and 12 days after the start of convection.

development, both features evolved differently. In a time-scale of one year, Clyde's Spot became a large and complex eddy, while the second storm transformed into a closed vortex (Hueso et al., 2022). A similar double-lobed morphology had been observed previously in a convective storm in a cyclone of the South South Temperate Belt (SSTB) observed by Voyager 2 in 1979, as the storm transformed into a large eddy in a time-scale of a few days (Fig. 1d) (Smith et al., 1979b; Hueso et al., 2022).

An additional storm that developed inside a closed cyclone was the eruption in the "STB Ghost" in February 2018 described in Iñurrigarro et al. (2020), which developed in a large and elongated cyclone (Fig. 1e). Numerical simulations of the convective storm in the STB Ghost presented by Iñurrigarro et al. (2020) reproduced the morphology of the evolution of the cyclone. Those simulations considered the interaction of convective pulses of different size, intensity and duration with the cyclone, and reproduced the overall evolution of the STB Ghost considering moist convective water storms with at least 1.0 times solar water abundance in the deep atmosphere (~5 bar). A recent study of water moist convection in another location in Jupiter with a complete implementation of a convective scheme on EPIC suggests water abundances of 2 times solar or less (Sankar and Palotai, 2022). Further evaluations of the possible deep water abundance required to drive large-scale storms were given by Hueso et al. (2002) from a study of a large storm originated in a small cyclone of the South Equatorial Belt (SEB) at the time of the Voyager 1 flyby in 1979 (Fig. 1f and g), with a possible value of 2.0 times solar water abundance. This range of values is consistent with more direct determinations of the deep water abundance from spectroscopic observations given by Bjoraker et al. (2018) of 1.1 times solar abundance near the Great Red Spot, and from Li et al. (2020) of $2.7^{+2.4}_{-1.7}$ for the equatorial latitudes from Juno data. Although Clyde's Spot was a much smaller storm than the storms in the SEB or the 2018 storm in the STB Ghost, it had an explosive outbreak that made us consider that this relatively small storm is a good candidate to gain insight into the deep water abundance of Jupiter.

Fig. 1 shows a summary of the convective systems introduced above, including the 1979 SEB outbreak, which was a convective eruption developing inside a cyclone but growing to a much larger size than the original cyclone.

Here we perform numerical simulations of Clyde's Spot and the similar storm formed at the same latitude in August 2021. We also perform simulations of the storm formed in the SSTB in 1979 and we investigate the characteristics of the cyclones and storms that built these perturbations exploring different initial vorticities and different values of the intensity of convection. These storms had in common their origin in a cyclone that survived the development of the convective storm and evolved over long time scales after convection ceased. Additional simulations of the 1979 storm in the SEB are also presented.

To run these simulations we use the Explicit Planetary Isentropic-Coordinate model (EPIC; version 3.81) (Dowling et al., 1998), modified to include the effects of convection through the addition of a heat impulse following García-Melendo et al. (2005). We compare our results for these storms with those already published for the STB Ghost (Iñurrigarro et al., 2020), and with the analysis of the SEB storm from Hueso et al. (2002). In addition, we also consider two alternative ways to introduce the effects of convective storms in EPIC with the aim to better quantify the energy released by the convective pulses that represent each storm. The comparison of our EPIC simulations of these storms allows us to establish a comparative scale of the energies associated to these convective events.

In section 2 we describe the EPIC model and our modeled atmosphere, vortex and storm initialization processes. We show the results of our simulations of cyclones and storms in the STB in section 3. We present our results for the storms observed by the Voyager spacecraft in the SSTB and the SEB in section 4. We discuss our results comparing the outcomes of our model with simulations presented in Iñurrigarro et al. (2020) and the study of the SEB storm in Hueso et al. (2002) in section 5. We summarize our results and present our conclusions in section 6.

2. The EPIC model

2.1. EPIC and initialization of vortices and storms

EPIC is the Explicit Planetary Isentropic-Coordinate atmospheric model (Dowling et al., 1998), a finite-differences model that solves the hydrostatic primitive equations under geostrophic balance using potential temperature, θ, as the vertical coordinate, and computes the evolution of potential vorticity, q. The latter is the magnitude used as a tracer of the flow, and is the one generally compared to the cloud morphology. Potential vorticity is defined as

$$q = \frac{\zeta + f}{\rho}\frac{d\theta}{dz} \tag{1}$$

where ζ is the relative vorticity determined by the wind field, f is the Coriolis parameter, ρ is the density, θ is the potential temperature, and z is the vertical Cartesian coordinate. This definition introduces the effects of the static stability of the atmosphere, through the $d\theta/dz$ term above. The potential temperature employed in EPIC is a mean of the potential temperatures of the constituents of the atmosphere, particularly the ortho and para hydrogen (see Appendix A in Dowling et al. (1998) for details). In addition, the potential temperature and pressure in a layer are computed from the values at the layers interfaces, which are calculated as the geometric mean over the interfaces with the definition in eq. (14) in Dowling et al. (1998).

The dynamics in EPIC include numerical diffusion with a hyperviscosity term used to control numerical instabilities. Here we use version 3.81 of the EPIC model, which unlike the EPIC implementation described by Sankar and Palotai (2022), does not include clouds, condensables and convection in an explicit way.

EPIC uses a longitudinal domain with periodic lateral boundaries in the zonal direction. The model domain is vertically bounded at the top with one or more sponge layers that attenuate the vertical reflection of gravity waves from the top of the atmosphere, and is bounded at the bottom with a deep abyssal layer representative of the adiabatic interior. The atmosphere is initiated with a vertical temperature profile, which determines the vertical stability of the atmosphere, and a zonal wind profile. The vertical structure of the winds can be added by imposing a multiplicative factor to the winds at different altitudes. From those sources of information, EPIC produces a simulated atmosphere under geostrophic balance in a configurable number of isentropic layers.

Vortices can be added in EPIC as Gaussian ellipsoidal perturbations of the Montgomery potential $M = C_pT + gz$ (Stratman et al., 2001; Legarreta and Sánchez-Lavega, 2008; Iñurrigarro et al., 2020), where C_p is the specific heat of the atmosphere, T is the temperature, g is the acceleration of gravity and z is the vertical coordinate. To add a vortex under geostrophic equilibrium EPIC uses the following perturbation of the Montgomery potential.

$$\Delta M = \alpha f R b_s V_T exp\left\{ -\left[\left[\left(\frac{\phi-\phi_s}{a_s}\right)^2 + \left(\frac{\varphi-\varphi_s}{b_s}\right)^2\right] + \left(\frac{ln(P)-ln(P_s)}{c_s}\right)^2\right]\right\} \tag{2}$$

Here $f = 2\ \Omega \sin \varphi_s$ is the Coriolis parameter, Ω is the planetary angular velocity, R is the local planetary radius, and V_T is the tangential velocity of the vortex, which is negative for cyclones. The parameters ϕ, φ and P are the east longitude, planetographic latitude and pressure respectively, and the sub-index s indicates the center of the vortex in each parameter. The size of the vortex is given by the semi-major and semi-minor axes a_s and b_s, and its vertical extent is measured in scale-heights with the parameter c_s. The parameter α is a non-dimensional number that depends on the distribution of velocities in the vortex through a shape-factor n following eq. (3).

$$\alpha = \frac{exp\left(1-\frac{1}{n}\right)}{n\left(1-\frac{1}{n}\right)^{1-1/n}} \tag{3}$$

Low values of n correspond to homogeneous distributions of vorticity, and higher values imply vortices with an outer annular structure. A standard value of n in most simulations of vortices in EPIC is $n = 2$.

When introducing vortices or other perturbations, this results in changes in the values of q that affect the elevations of the isentropes in a way related with the static stability of the atmosphere at each layer. Vortices with very large tangential velocities over small areas require strong gradients of pressure that are different at different depths. These vortices produce vertical motions that occur adiabatically over isentropes. However, this means that strong and small vortices deform the isentropic layers to the point where, due to model limitations, isentropes can cross each other. This makes the model to collapse due to θ not being a monotonic function of altitude and multi-valued variables at the grid points where the isentropes cross. For the size of the smaller vortices simulated in this work and the tested tangential velocities, this occurs for tangential velocities of 100 ms^{-1}. Also, the initial vortex quickly evolves interacting with its environment achieving geostrophic conditions in the environment and the vortex.

Storms are introduced similarly by adding heating sources with Gaussian heat pulses $\dot{Q}$ that can be active for a prescribed time. Following García-Melendo et al. (2005) heating sources are introduced as

$$\dot{Q} = \dot{Q}_0 exp\left(-\left(\frac{(\phi-\phi_0)^2}{2a^2} + \frac{(\varphi-\varphi_0)^2}{2b^2} \right) \right) \tag{4}$$

where $\dot{Q}_0$ is the intensity of the pulse measured in units of power per mass (Wkg^{-1}) and $\phi_0$and $\varphi_0$indicate the east longitude and planetographic latitude of the storm. In this equation a and b are a measure of the longitudinal and latitudinal size of the convective pulse. The combination of storm intensity ($\dot{Q}_0$), size (a, b), and duration of heating are related in a direct way with the total energy injected in the storm, and the parameters $\phi_0$and φ_0 allow to inject the storm in any location of the model domain. Convective pulses deform the isentropes progressively as their effects accumulate in time while the storm is active. This means that there are practical limits to the maximum intensity of the storms that can be simulated. For instance, very intense pulses with values of 5 Wkg^{-1} result in isentropes that cross each other in time-scales of about 0.2 days rendering the model unstable. Smaller values of $\dot{Q}_0$ prolonged over long time-scales can also render the model unstable, but in general the upper limit of energy that can be simulated also depends on the size of the pulse and vertical resolution of the model.

Several studies of convective storms following this scheme have been done for Jupiter (Sánchez-Lavega et al., 2008, 2017; Iñurrigarro et al., 2020) and Saturn (García-Melendo et al., 2013; Sánchez-Lavega et al., 2020). Those studies do not attempt to reproduce how convection starts, but rather the response of the atmosphere to different convective events introduced in the model. In particular, in our previous study of the 2018 storm in the STB (Iñurrigarro et al., 2020) we used EPIC to simulate the storm onset and its interaction with the elongated cyclone where the storm formed using exactly this approach and reproducing the morphology of the elongated cyclone after the storm ceased to be convective. Realistic simulations that reproduced the observations were achieved well below the limit of maximum convection that the model can simulate.

The heating source defined in eq. (4) acts over the interfaces between the different isentropes following eq. (31) in Dowling et al. (1998). When introducing convective pulses, eq. (4) acts as a mass source that locally modifies the vertical structure of isentropes (García-Melendo et al., 2005). However, the implementation of that equation in García-Melendo et al. (2005) and later works introduces the convective pulse in all the interfaces of the model, and so, it introduces energy in all vertical layers, except in the abyss where the pulse is not introduced, and in the upper sponge layers that quickly dissipate the pulse. This provides stability to the simulations by modifying similarly the different isentropes but it is problematic when comparing to how moist convection operates in a real atmosphere. In a water moist convective storm, when water condenses at pressures around 5 bar, it warms the local air and produces an updraft that ascends until it reaches the upper troposphere where the static stability of the atmosphere decelerates and ultimately stops the vertical motions (Stoker, 1986; Hueso and Sánchez-Lavega, 2001). The result is that convection transports energy from the water condensation level to the layers where static stability grows and the updrafts are decelerated producing divergent motions. These levels are located from around 1 bar to the uppermost levels reached by the storm. When convection ends, the lower levels have similar temperatures to their original state, except that they do not have water vapor to feed more convection. The result is that the upper atmosphere has been warmed over large areas from the divergence at the upper clouds, but not the lower atmosphere from where latent heat has been extracted. Thus, observations of the upper cloud fields allow basic estimations of energy from the size of the expanded cloud system combined with reasonable hypothesis of the heating produced by convection (Banfield et al., 1998; Hueso et al., 2002). Because in EPIC we do not simulate how convection forms, but rather how the atmosphere reacts to the consequences of convection, an alternative to the way previous EPIC simulations of storms have been done is to introduce the heating source only in the interfaces of the layer (s) where convection deposits energy in the upper troposphere. We will evaluate the impact of both alternatives when initiating convective storms.

2.2. Model atmosphere and model domain

We use a vertical temperature profile from Voyager that is extrapolated to the lower atmosphere following a pseudoadiabat with ammonia and water and assuming an homogeneous deep abundance of condensables of 2.7 times solar values for ammonia, hydrogen sulfide and water. These values are used from the recent derivation of deep ammonia in Jupiter's atmosphere at all latitudes and the water abundance in Jupiter's equatorial region obtained by the Juno mission (Li et al., 2017, 2020). The vertical gradient of condensables introduces static stability in the bottom layers of the model domain. Zonal winds are introduced at cloud level using the 2016 HST and amateur zonal wind profiles from Hueso et al. (2017) updated with 2017 HST and amateur data, and we consider constant winds at all altitudes. An examination of the vertical shears expected from thermal winds measured from Cassini data and ground-based observations (Fletcher et al., 2016) suggests that vertical shears are negligible at the STB above the cloud level, a point that we specifically tested and confirmed in numerical simulations of vortices in the STB. For simulations of the Voyager storm in the SSTB and the SEB we used the Voyager zonal winds from Limaye (1986). The geostrophic equilibrium condition requires the model to compute minor corrections to the vertical thermal structure, a step that is done by EPIC at model initialization after introducing the vertical thermal structure and the zonal winds.

Our simulations of Clyde's Spot are run over a longitudinal channel of 40 or 80° and 10° in latitude with periodic boundaries in the zonal direction. The spatial resolution of these simulations is either 0.04° per grid point, which are restricted to longitudinal domains of 40°, or 0.08° per grid point in experiments using the longitudinal domain of 80°. The simulations extend from 10 mbar to 7 bar in the vertical direction with 8 layers, where the 8th layer represents the abyssal atmosphere below 7 bar considered to be adiabatic. The top two layers are modified to behave as "sponge" layers that attenuate reflected gravity waves from the top of the model. Fig. 2 shows the vertical structure of the modeled atmosphere (the abyssal layer is not shown). Slightly different domains are used when simulating other storms and Table 1 gives a summary of

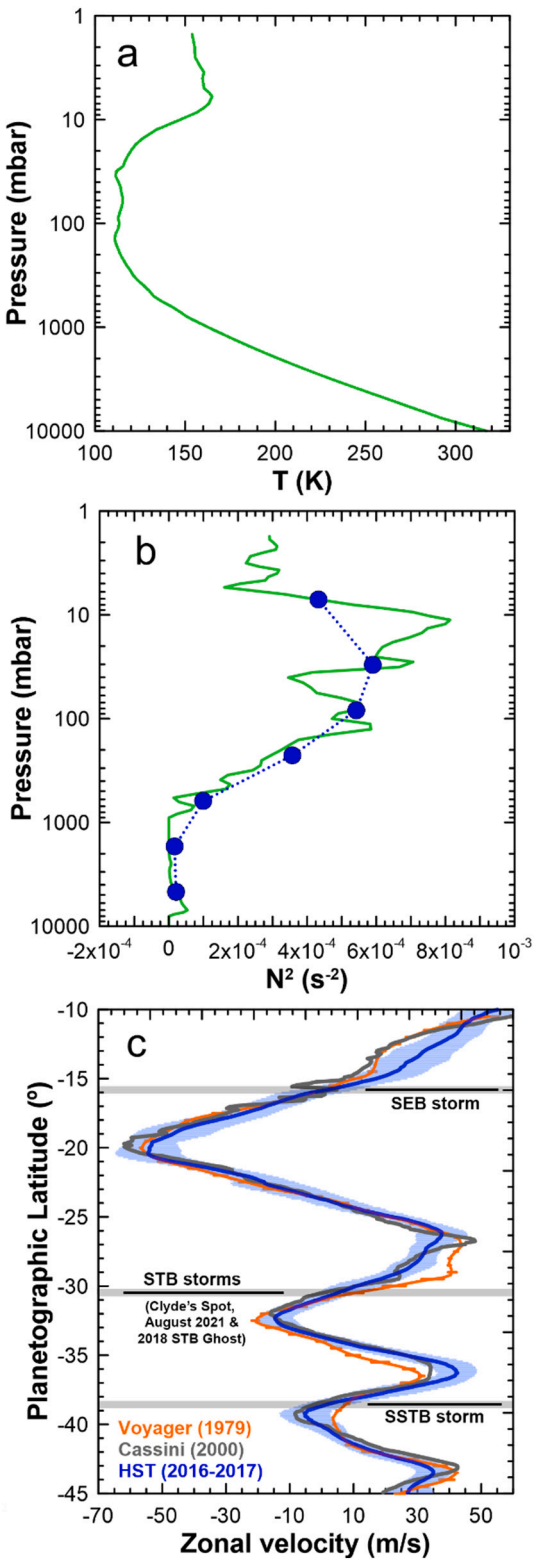

Fig. 2. Model atmosphere used in EPIC. (a) Vertical thermal profile and its extrapolation to the lower levels following a moist pseudoadiabat assuming 2.7 solar abundances of condensables. (b) Squared Brunt-Väisällä frequency ($N^2 = g/\theta\ d\theta/dz$) of the atmosphere (green), and values used by EPIC in its 8 layers (blue dots; the abyssal layer is not shown) (c) Zonal winds used in the model domain are either those from HST and amateur measurements (blue line, 2016–2017) or those characteristics of the Voyager 1 and 2 flybys for the simulations of the Voyager 2 cyclonic storm (orange, Limaye, 1986). The winds are considered to be constant at all depths in the simulated domain. The zonal winds measured at the time of the Cassini flyby from Porco et al. (2003) (grey line) are also shown as a reference. Voyager and HST are shown with their respective error bars. Horizontal lines in (c) show the latitudes of the storms under study. (For interpretation of the references to colour in this figure legend, the reader is referred to the web version of this article.)

the parameters defining the domain and spatial resolutions used in different sets of simulations. These are: (*i*) vortices merger in the STB, (*ii*) storms in cyclones in the STB, (*iii*) the convective cyclone observed by Voyager 2 in the SSTB, (*iv*) the convective storm observed by Voyager 1 in the SEB.

We use an adaptive time step that fulfils the numerical stability conditions required by the EPIC model. These include requirements given by the hyperviscosity ν_6 scheme used in EPIC (Dowling et al., 1998) and the classical Courant CFL condition. However, when exploring the simulated velocity fields we found that minor numerical instabilities in the form of a fine-grain structure developed in the simulation. This noise was not discernible in the potential vorticity maps in simulations with a resolution of 0.08° per grid point, but was slightly noticeable in the ones with 0.04° per grid point, and was a source of noise in plots of zonal velocities, u, or meridional velocities, v. These small-scale instabilities are eliminated when running the simulation with a time step of 0.25 times the Courant CFL condition. This results in typical time steps of 6 s for the simulations with a resolution of 0.08° per grid point and 3 s for the simulations with a resolution of 0.04° per grid point.

We do not treat here the possible interaction of the STB cyclones with the Great Red Spot described in Hueso et al. (2022) due to limitations of the model. The simulation of convective storms in small cyclones requires a combination of high-resolution and small time step and that interaction extended over tens of days. For comparison, the 0.04° per grid point spatial resolution used in many of the simulations of Clyde's Spot presented here, is 4 times smaller than the simulations done to study the convective outbreak in the STB Ghost in Iñurrigarro et al. (2020) and 4 times smaller than EPIC simulations of the GRS presented in Sánchez-Lavega et al. (2021). Time steps used here are 3 times smaller than those in Sánchez-Lavega et al. (2021), and simulating the interaction of cyclones, storms and the GRS would require an order of magnitude of increased computational power. In addition, similar storms observed in closed cyclones, like the ones ocurring in 2018 in the STB Ghost and the 1979 storms in the SEB and SSTB observed by Voyager 1 and 2 did not interact previously with large scale features, and it is unclear from an observational point of view if this is an important element of the convective storms in the STB.

3. Numerical simulations of convection in closed cyclones in the STB

3.1. Cyclones mergers in the STB

Clyde's Spot developed in a cyclone that had formed from a merger of two smaller cyclones. The same occurred with the storm in August 2021. Since cyclones are regions of low pressure at cloud level,

Table 1
Domain and resolution used in the simulations of vortices merger, Clyde's Spot in the STB and the 1979 storms in the SSTB and SEB observed by Voyager 2 and Voyager 1 respectively.

Parameter	STB vortices merger	STB storm	SSTB storm	SEB storm
Latitudinal range (°)	−35 to −25	−35 to −25	−44 to −34	−25 to −5
Longitudinal range (°)	−40 to 40	−20 to 20 or −40 to 40	−40 to 40	−40 to 40
Altitude range (mbar)	10 to 7000	10 to 7000	10 to 7000	10 to 7000
Number of layers	8	8	8	8
Resolution (°/pixel)	0.08	0.04, 0.08	0.08	0.08

isentropes in cyclones ascend in the deeper layer and descend in the upper layers. The ascending structure of their bottom layers may favor the development of moist convection, an idea presented in the literature several times to relate cyclonic shear and moist convection in Jupiter (Dowling and Gierasch, 1989; Thomson and McIntyre, 2016; Fletcher et al., 2017). Here we explore if the vertical structure of a cyclone obtained after merging previously existing cyclones can enhance these characteristics favoring the development of moist convection.

We introduce 2 vortices separated in longitude by about 15° and in latitude by different distances always smaller than 0.15°, but large enough to produce different drift rates for each cyclone. The vortices have a semi-major longitudinal size of 0.7° and a semi-minor latitudinal size of 0.6° from values estimated from the sizes of observed STB cyclones. The vortices are assumed to extend 3 vertical scale heights above and below a vortex mid-plane centered at the cloud level at 680 mbar. This vertical extension is taken from previous simulations in Iñurrigarro et al. (2020) of Oval BA, the STB Ghost and other features in the STB. However, since the zonal winds are assumed to have no vertical wind shear below the visible cloud level (also an assumption from extensive simulations of features in the STB and other latitudes in Jupiter in previous works), the simulations are not sensitive to the true vertical extension of the cyclones. The radial distribution of velocities in these vortices is fixed by using $n = 2$, which is a standard value for most vortices, except for large vortices where rings of vorticity can be resolved, like in Oval BA or the GRS. We did not test different values of n because of the small size of our vortices. Table 2 shows the range of the parameters explored in simulations of vortices merger in the STB.

The mean tangential velocity of Clyde's Spot was 30–50 ms^{-1} from measurements in Hueso et al. (2022). Here we tested values of the tangential velocity of the vortices before convection (25, 50 and 75 ms^{-1}). Attempts to run simulations with higher tangential velocities (100 ms^{-1}) result in instabilities due to the large vorticities implied in such small cyclones. Those high vorticities deform isentropes so strongly, that isentropes cross each other making the model to collapse. We also run preliminary simulations with different non-zero vertical shears of the zonal winds. Small vortices like those simulated here are vertically sheared apart by the different winds at different altitudes. This result was found even when simulating vortices with strong tangential velocities of 75 ms^{-1}. Thus, we considered no vertical shear in the STB in agreement with thermal winds presented in Fletcher et al. (2016), and also in agreement with the detailed exploration of parameters of the atmosphere at the STB in Iñurrigarro et al. (2020).

Table 2
Explored range of the parameter space to model the merger of vortices in the STB. ϕ_s is the east longitude, φ_s the planetographic latitude, a_s the longitudinal semi-mayor axis, b_s the latitudinal semi-minor axis, V_T the tangential velocity of the vortex, P_S the reference pressure level where the vortex center is located, C_{up} the vortex upward extension, C_{down} the vortex downward extension, and n the shape-factor.

Parameter	Vortex 1	Vortex 2
ϕ_s (°)	−20.0 to −8.0	0.0
φ_s (°)	−30.40 to −30.55	−30.55 to −30.70
a_s (°)	0.7	0.7
b_s (°)	0.6	0.6
V_T (m s^{-1})	−25, −50, −75	−25, −50, −75
P_s (mbar)	680	680
C_{up} (scale heights)	2, 3	2, 3
C_{down} (scale heights)	3	3
n	2	2

The vortices are introduced at the latitudes measured in Hueso et al. (2022) and reproduce the observed drift velocities. In almost all of our simulations the two vortices exhibit regular oscillations in latitude resulting in non-constant zonal drift rates similarly to the behavior observed for the STB cyclones. Fig. 3 shows the results of one of our simulations for vortices with a tangential velocity of 50 ms^{-1}. When the two vortices approach closer than ~6° they start to interact, modifying their previous zonal drift for about 10 days and merging together in a stable vortex in a process that lasts about 6 days for an homogeneous mixing of the two vortices that does not produce external turbulence.

Very similar results are obtained when simulating vortices with different tangential velocities from 25 to 75 ms^{-1} with no major differences in the merger process. We conclude that cyclones in the STB merge easily, forming stable structures without producing additional turbulent patterns. Thus, the capacity of these simulations to provide an indication of the cyclones circulation is small, and the case shown in Fig. 3 with a tangential velocity of 50 ms^{-1} can be considered as fully representative of the three simulations.

The regular decrease of potential vorticity in the simulations observed in Fig. 3 from day 1 to 90 is mainly caused by numerical diffusion and hyperviscosity, with a slight decay of peak values of the potential vorticity of ~20% during the merger of both vortices.

The new cyclone created by the merge of the two initial vortices is larger by about a factor of 1.9–2.1 in area when compared with the vortices on day 65. In the case shown in Fig. 3 its outermost tangential velocity peaks at 50 ms^{-1}, suggesting a similar tangential velocity after the merger to the initial vortices, and similar but slightly smaller potential vorticity.

We also used these simulations to explore what are the effects of the cyclones merge in their vertical structure through the modification of the isentropic surfaces. Fig. 4 shows a comparison of the vertical deformation in the isentropes caused by the structure of the cyclones through longitudinal cuts on days 60 (with two cyclones separated in longitude) and day 110 (well after both cyclones merge).

Changes in the values of q affect the elevations of the isentropes in a way related with the static stability of the atmosphere at each layer (see eq. 1). Thus, vertical deformations of the isentropes associated to the vortex are small in the upper troposphere and large in the deep atmosphere where static stability drops. The new vortex induces a slightly larger perturbation at all levels, but the upper troposphere at 230 mbar is not well represented, being close to the sponge layer where significant filtering affects the model. The vertical structure of the vortex after the merger of the cyclones is enhanced at intermediate layers (620 and 1700 mbar), where static stability is large or moderate, but changes in the lower atmosphere at 5 bar, where static stability is smaller, are not particularly noteworthy at the isentrope close to the water condensation layer.

The simulations and the structures shown in Fig. 4 suggest that the result of the vortex merger has a limited but non-null capacity to enhance the uplift of material from deeper layers, which are potentially richer in water. Atmospheric conditions with lower stability at the water condensation layer than those here simulated might produce bigger perturbations on the isentropes at those levels, further favoring the development of vertical motions.

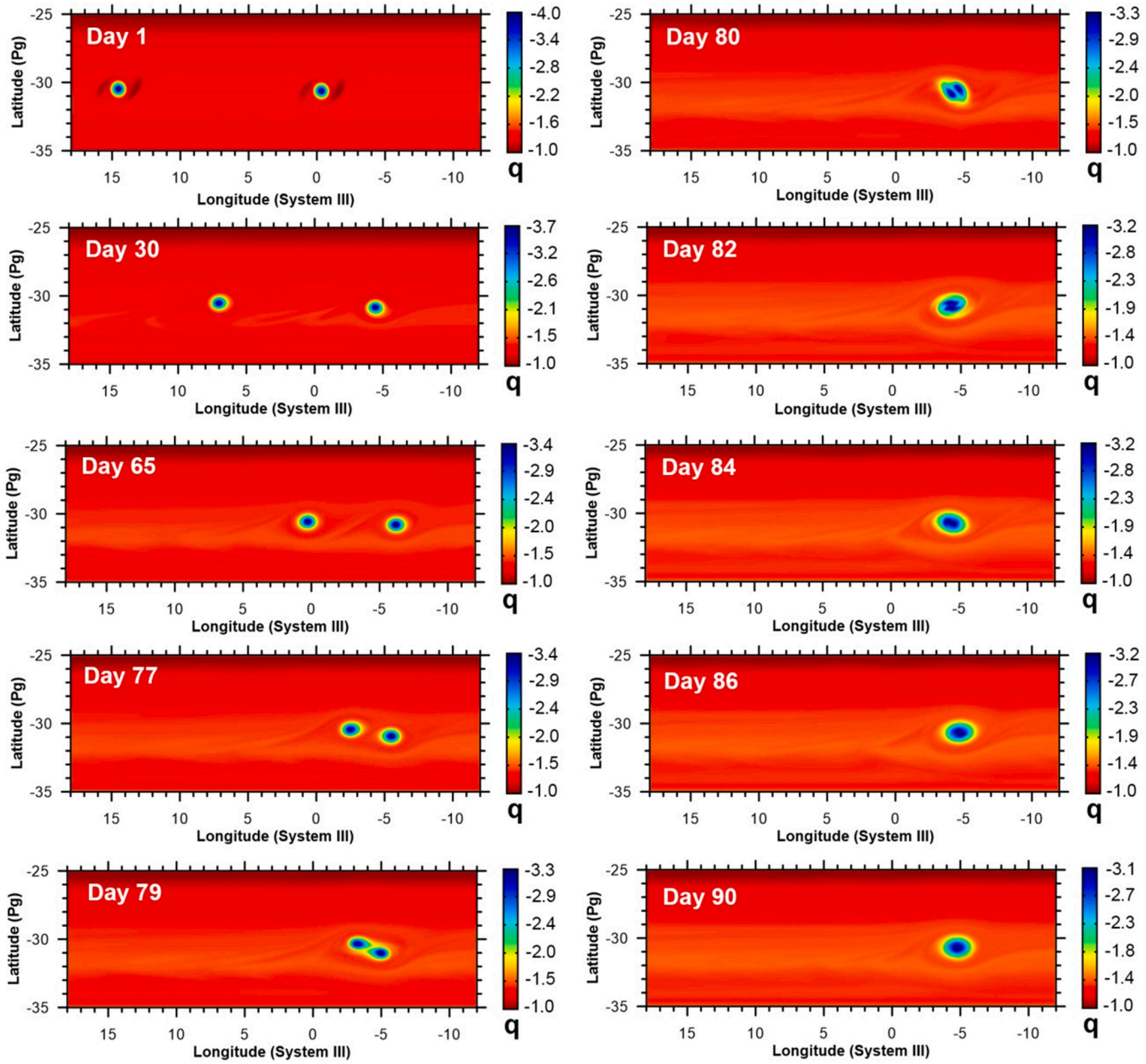

Fig. 3. Potential vorticity (q in units of 10^{-6} m^2Ks^{-1} kg^{-1}) of a simulation of the cyclones merger for two cyclonic vortices with tangential velocities of 50 ms^{-1}. The dark structures around the two vortices on day 0 are small perturbations created in the atmosphere by the artificial introduction of vortices in EPIC and dissipate quickly. Left column: vortex drifting and mixing. Right panels: merger and final stable vortex. This simulation had a spatial resolution of 0.08° per grid point.

3.2. Convective storms in the STB cyclones: Short-term evolution

We now explore the evolution of small cyclones in the STB when a short-lived convective storm develops in their interior. The simulations show a complex interplay between the parameters that define the vortices and those that define the convective pulse. Tables 3 and 4 summarize the range of values explored. We also give equivalent parameters for the simulations of the SSTB and SEB storms observed by Voyager 2 and Voyager 1 in 1979 and discussed in section 4.

We first initialize a cyclone with semi-major axis of 1.5° and semi-minor axis of 1.1°. These sizes correspond to the cyclones where Clyde's Spot and the August 2021 STB storm developed. We consider tangential velocities of 25, 50 and 75 ms^{-1} to initialize the vortex. The simulations evolved for 26 days to spread small-scale instabilities from the vortex initialization process before introducing a convective pulse at the center of the cyclone with different heating intensities.

The drift rate of the convective pulse was selected to match the cyclone's drift rate. We run simulations with different sizes of the pulses. Convective pulses that are sustained over areas that are larger than the original cyclone destroy the cyclone quickly, contrarily to what observations show. Small pulses with radius $a = 0.2°$ are not big enough to disturb the vortex meaningfully and require very high intensities if they are settled to produce an energetic event capable of significantly transforming the cyclone. To reduce the number of parameters we fixed the size of the convective pulse to a radius of $a = 0.5°$, which is slightly smaller than the original observation of Clyde's Spot, and is similar to the sizes used in our simulations of the convective storms inside the STB Ghost in 2018.

We considered a single convective pulse of short duration in agreement with the observed evolution of the storm in methane band images,

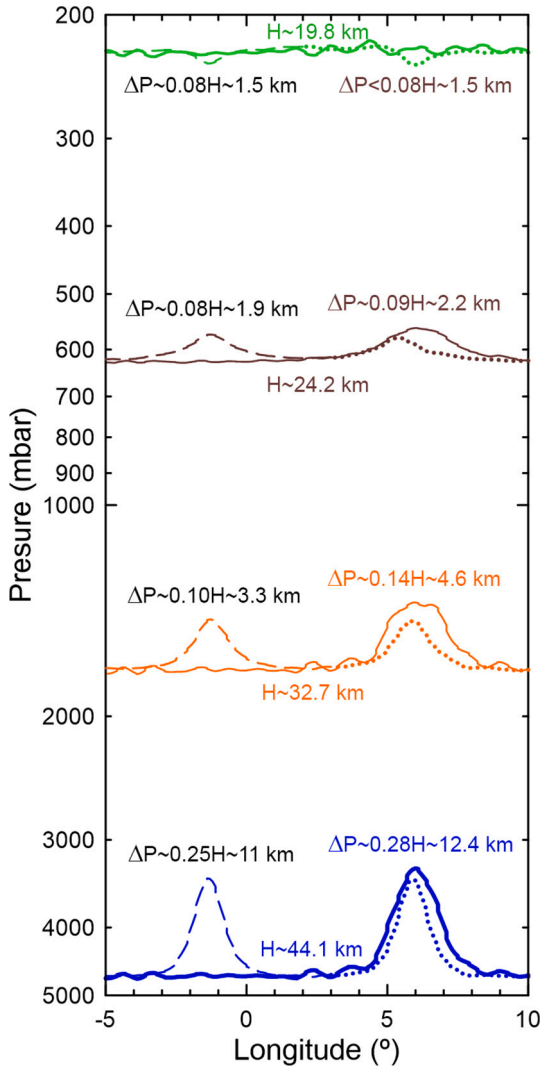

Fig. 4. Vertical structure of isentropes in the cyclones. Lines represent longitudinal cuts of the cyclones obtained at the central latitude of the vortices. Dotted and dashed-lines represent the two cyclones on day 60 of the simulation. Continuous lines represent the result of the merge on day 110. The vertical extension of the perturbation induced by each cyclone is shown for one of the vortices on day 60 and for the result of the merge. Insets show the perturbation of pressure ΔP associated to each layer in terms of vertical scale heights *H*. Black insets on the left are for the original vortices, colored insets on the right represent those of the merged cyclone. Insets give information on scale heights and vertical changes in the structure of the vortices.

Table 3
Parameter space of simulated vortices.

Parameter	STB cyclones	SSTB cyclone
φ_s (°)	−30.5 to −30.6	−38.5 to −39.1
a_s (°)	1.5	4.05
b_s (°)	1.1	1.7
V_T (m s^{-1})	−25, −50, −75	−30
P_s (mbar)	680	680
C_{up} (scale heights)	2, 3	3
C_{down} (scale heights)	3	3
n	2	2

with a sudden apparition and less intense bright features in the next Jupiter rotation (Fig. 4 in Hueso et al., 2022). We introduced convective pulses following the two approaches described in section 2.1. We first introduce a heat pulse that affects the full vertical structure of the atmosphere (except the deep abyss) with a given value of $\dot{Q}_0$. This procedure is comparable to the one used in Iñurrigarro et al. (2020) for their study of the 2018 storm in the STB Ghost. We then replicate those simulations with a heat pulse that is only introduced in the interface between the isentropes at 620 and 1700 mbar. We first describe the simulations for a convective pulse affecting the full vertical structure of the atmosphere.

Table 4
Parameter space of simulated convective storms.

Parameter	STB storm (Clyde's Spot and Aug. 2021 storm)	SSTB storm (Voyager 2)	SEB storm (Voyager 1)
φ_0 (°)	−30.5 to −30.8	−38.2 to −39.4	−16.5 to −15.2
a (°)	Tested: 0.2 to 0.8, nominal = 0.5	Nominal = 0.8	0.15 to 1.0
b (°)	0.2 to 0.8	0.65	0.15 to 1.0
Drift rate (m s^{-1})	2	7	−6.9 to 8.5
Start time (days)	25, 26	30	0
Time active (days)	0.25, 0.75, 1, 1.5, 2.0	0.5, 0.75, 1.0	4, 7
$\dot{Q}_0$ (Wkg^{-1})	0.2 to 5.0	0.3 to 1.0	0.5 to 3.0

3.2.1. *Short-term evolution with vertically extended heat pulses*

Simulations of short convective pulses demonstrated that the initial cyclone can be broken in two side-lobes similar to the Junocam observation 2.5 days after the storm onset. After testing several values of the duration of the convective pulse, we fixed this parameter to 0.25 days. The rationale for this specific time-scale is that storms that are active for a longer period of time (0.75 days or longer) produce long standing features that rotate inside the vortex without ever forming a double-lobed structure as the one observed by Junocam or the one also observed for the August 2021 storm (Fig. 1). This time-scale is also supported by the observations that showed a quick apparition and fast demise of activity in the methane band images in just a few Jupiter planetary rotations (Figs. 4 and 8 in Hueso et al., 2022).

We performed a battery of simulations with different tangential velocities of the vortex and different intensities of the convective heat pulse. We also run simulations with no vortex but similar heat pulses to explore the response of the atmosphere to events of pure convection with no initial vortex. Fig. 5A shows the vortex-storm structure at the isentrope with average pressure of 620 mbar 3 days after the onset of the storm, a time-scale comparable to the Junocam images of Clyde's Spot.

Fig. 5A is organized with rows showing results for different tangential velocities of the vortex and columns showing results with different intensities of convection. The upper row in Fig. 5A shows the results of simulations of pure convective storms formed without a pre-existing cyclone. These simulations produce anticyclonic structures that are torn apart by the environment cyclonic winds. If the storm is powerful enough, $\dot{Q}_0$=2.0 Wkg^{-1}, then the anticyclone is stable on time-scales of a few days and migrates slightly northward as a consequence of its interaction with the environment cyclonic winds.

The second row in Fig. 5A shows results for weak cyclones with tangential velocities of 25 ms^{-1}. These cyclones confine the region affected by weak convection, but can break apart easily in two sides with moderate heat pulses (0.5 Wkg^{-1}), being completely broken for intense heat pulses (1.0 Wkg^{-1}). The long-term evolution of these vortices however, shows clear dissipation and they do not seem to reproduce the observed characteristics of the long-term evolution of the dark remnant of Clyde's Spot. Simulations of very intense convective pulses inside these weak cyclonic vortices (right side of the second row in Fig. 5A) with $\dot{Q}_0$=2.0 Wkg^{-1} are similar to the storms simulated without first introducing a cyclone, and show that an intense convective pulse can

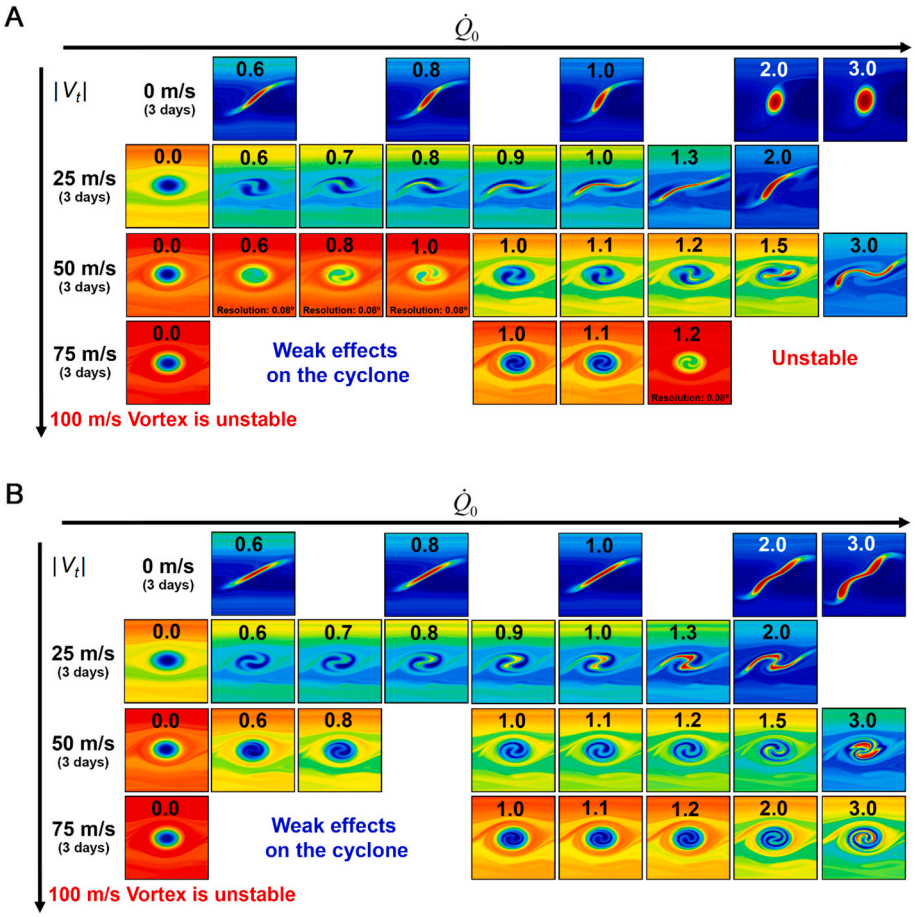

Fig. 5. A: Exploration of the vortex-storm parameter space when introducing vertically extended heat pulses. From top to bottom vortices of different tangential velocities. From left to right storms of different intensities. Subpanels show a small subsection of the potential vorticity field at the mean 620 mbar level. The magnitude of the heat pulse that represents the storm appears as a number (units of Wkg^{-1}) in each panel. All panels are taken at 3 days after the storm initialization. Most of these simulations were run with a spatial resolution of 0.04° unless otherwise stated in the legend inside individual subpanels.
B: Same as A but for convective pulses introduced as vertically limited heat pulses in the interface between isentropes with average pressures of 620 and 1700 mbar.

break a cyclone completely.

Intense vortices with tangential velocities of 50 ms^{-1} confine the effects of the storm better (third row in Fig. 5A). These simulated cyclones break apart in two sides, but require more intense convection with heat pulses of 0.8–1.2 Wkg^{-1}. These cases show a better comparison with the observations of the short-term evolution of Clyde's Spot and the August 2021 storm. Among the different cases shown in Fig. 5A, convective pulses of 1.0–1.2 Wkg^{-1} generate morphologies similar to the double-lobed structure observed in the Junocam image of Clyde's Spot (Fig. 1b).

Finally, very intense vortices with tangential velocities of 75 ms^{-1} are difficult to perturb with convective pulses (fourth row in Fig. 5A). The convective pulse forms structures in the cyclone that are reminiscent of structures observed in Clyde's Spot, but they mix together very rapidly in spiral patterns that are very different to what the observations show only a few days after the active storm dissipates. Very intense heat pulses are necessary to break the cyclone in a two lobed structures, but the model becomes unstable for heat pulses larger than 1.2 Wkg^{-1} in these intense vortices. Thus, it seems very unlikely that the original cyclone had the intense tangential velocities here used as an initial condition for the vortex.

From the simulations shown in Fig. 5A we considered the case with a vortex with a tangential velocity of 50 ms^{-1} and a storm with a heat pulse of 1.0 Wkg^{-1} as our nominal case. This is the most successful in terms of its morphological comparison with the Junocam observation of Clyde's Spot (Fig. 1b) and amateur observations of the August 2021 STB convective event (Fig. 1c).

3.2.2. *Short-term evolution with vertically limited heat pulses*

Fig. 5B represents the same simulations as Fig. 5A, but now using heat pulses that are introduced only in the interface between isentropes with average pressures of 620 and 1700 mbar. For the same values of $\dot{Q}_0$ the amount of energy introduced in the simulation is now smaller, but the energy introduced in the observable levels at around 600 mbar are similar, making the apparent results of both sets of simulations roughly similar. Since the energy is introduced in the interface between two isentropes, the vertical structure of the system is strongly affected at those two levels and is only slightly modified in the layers above and below. For instance, if we just concentrate in the first row of Figs. 5A and B showing simulations without an initial cyclone, the convective pulses introduced previously are vertically extended through the atmosphere and develop vertically coherent anticyclones that interact with the cyclonic winds (Fig. 5A). However, when convective pulses are vertically limited, the anticyclonic systems formed by convection are shallower and are easily torn apart by the environment winds (Fig. 5B).

From the simulations in Fig. 5B we consider that the case with a vortex with a tangential velocity of 50 ms^{-1} and a storm with a heat pulse from 1700 to 620 mbar of 1.2 Wkg^{-1} is the closest one to our previous nominal case (a convective pulse of the same size and duration, with a power of 1.0 Wkg^{-1}, introduced all the way from the lowest layer above the abyss to the sponge layer).

Fig. 6 compares the vertical structure of the atmosphere at the center of the cyclone for the two simulations that have been chosen as the nominal ones in which energy is introduced either extended over the atmosphere (except the abyss) as in the simulations shown in Fig. 5A, or in a single interface between two isentropes as in the simulations in Fig. 5B. The figure shows the effects of convection over the free atmosphere (i.e. without a previously existing cyclone), or when introducing a convective pulse inside a cyclone. Since energy is introduced as a mass source, isentropes above and below the region modified are deformed,

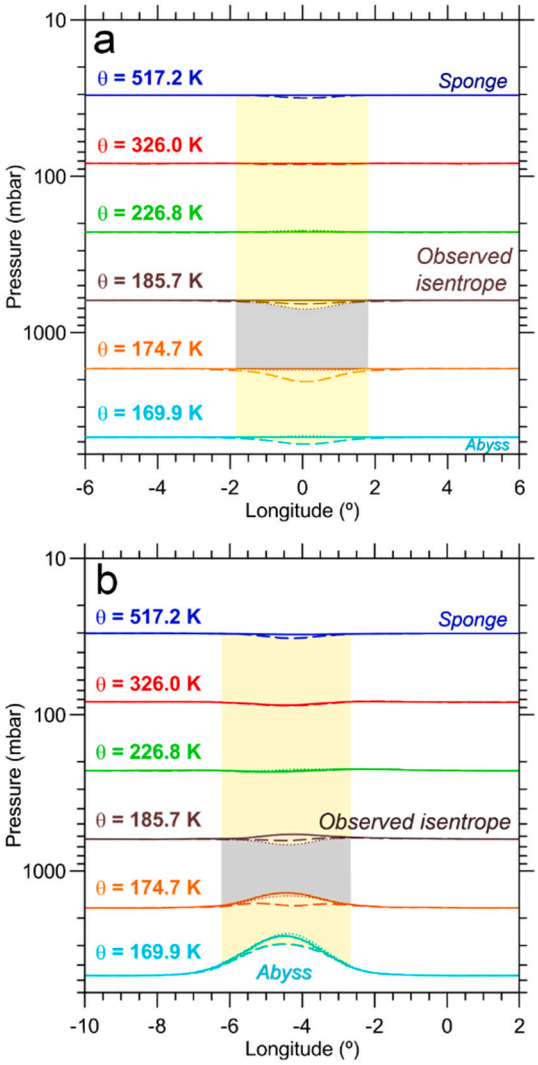

Fig. 6. Vertical structure of isentropes for the two storm initialization schemes. (a) Isentropes in a model atmosphere without cyclones and in which a convective pulse has been introduced. Solid lines represent the isentropes in the initial atmosphere without the convective perturbation. The dashed-lines and yellow-shaded area show the isentropes and region perturbed when introducing a convective pulse of 1.0 Wkg^{-1} vertically extended over the atmosphere. The dotted-lines and grey-shaded region represent the effects of introducing a convective pulse of 1.2 Wkg^{-1} only in the interface between the isentropic layers with $\theta = 175$ K and $\theta = 186$ K, equivalent to pressure levels of 620 to 1700 mbar outside the perturbation. (b) Same as (a) but in a simulation in which the convective pulse has been introduce at the center of a cyclone with $V_T = 50$ ms^{-1}. Solid lines show the isentropes for the cyclone only. The dashed lines and yellow-shaded area show isentropes for the cyclone after introducing a convective pulse of $\dot{Q}_0 = 1.0$ Wkg^{-1} extended over the atmosphere. The dotted lines and grey-shaded area correspond to a convective pulse of $\dot{Q}_0 = 1.2$ Wkg^{-1} introduced only in the shaded grey region between the two isentropes with mean pressures at 620 and 1700 mbar. In both panels the time shown is two hours after the convective pulse of 0.25 days ends. (For interpretation of the references to colour in this figure legend, the reader is referred to the web version of this article.)

and whether we inject energy in all the model interfaces or in a single model interface, all the isentropes are affected. However, in both cases the vortex structure is mostly affected at the isentrope with mean pressure of 620 mbar, which lies at the top of the interface where we introduce our convective pulse in the second convective scheme. Since in both convective schemes we introduce similar amounts of energy close to the isentrope that represents the upper cloud layer, the outcome of the simulations is relatively similar. Thus, the differences in potential vorticity at cloud level shown in Figs. 5A and B are relatively small. However, the vertical structure of the vortex-storm system is different in both sets of simulations and the long-term evolution of both sets of simulations can be different too.

We conclude that both convective schemes (a vertically extended pulse or a shallower convective pulse close to the visible cloud level) produce similar results in terms of the morphology at the cloud visible level. However, a detailed calculation of the absolute energy introduced in the model, while numerically possible, might not be physically meaningful, since two very different energy inputs can result in similar evolutions of the nearest layer to the visible cloud level. This means that the simulations cannot directly distinguish how much condensation of water should be needed to reproduce Clyde's Spot and other convective storms from the energy introduced in the model (e.g. Iñurrigarro et al., 2020). However, a relative evaluation of the different energy involved in simulations of different storms can be more appropriate. Nevertheless, for Clyde's Spot and the 2021 STB storm, an approximate simple calculation of the required local water abundance in these storms could be performed considering the heating amplitude and the duration of the heat pulse.

3.3. Mid-term evolution of the nominal case

Details of the short and long-term evolution of the storm-vortex system for the two nominal cases selected above are shown in Fig. 7. The leftmost two columns show the evolution of the cyclone with a convective pulse of 1.0 Wkg^{-1} introduced all through the atmosphere. The rightmost two columns show the evolution of the cyclone with a convective pulse of 1.2 Wkg^{-1} introduced only in the interface between the two isentropes with pressures of 620 and 1700 mbar. In both cases, the convective pulse is active over 0.25 days and acts as a divergence source that separates the inner part of the cyclone in two sides quickly. These two sides rotate clockwise with an approximate period of 3 days, while the outer part of the vortex is not strongly affected by the storm. After ~6 days, patches of strong cyclonic vorticity are concentrated in the inner core of the vortex outside of its center and can be seen to rotate clearly. We consider that these features ("dark blue" in the image of the simulation, and thus, more cyclonic than their environment) compare well with dark patches observed in Clyde's Spot, forming inside the vortex in its transition from the bright storm into the dark remnant, and possibly representing cloud clearings. A ring of almost unperturbed material separates the inside perturbed region from the outside, keeping the size of the vortex almost constant. In both cases, 20–30 days are needed to homogenize the interior of the vortex, which keeps a very different structure to the initial vortex.

3.4. Mid-term evolution of storms of varying intensity

We also run the simulations shown in Figs. 5A and B with longer times to investigate their mid-term evolution. Results for storms initiated inside cyclones with different initial tangential velocities of 25 and 50 ms^{-1} are shown in Fig. 8 in simulations performed with a spatial resolution of 0.08°. We show results for the two convective schemes introduced before.

The upper two rows of Fig. 8 show results for weak vortices ($V_T = 25$ ms^{-1}). Vortices perturbed with weak convective pulses ($\dot{Q}_0 \sim 0.6$ Wkg^{-1}) almost do not show inner structures after 25 days. The same vortices perturbed with strong convective pulses ($\dot{Q}_0 \sim 1.8$ Wkg^{-1}) are destroyed leaving highly turbulent structures. Convective pulses with energy distributed vertically over the atmosphere (columns b_1 and b_2 in Fig. 8) are more energetic than convective pulses only affecting the interface between two isentropes (columns c_1 and c_2 in Fig. 8), and so, the latter cases are less perturbed for intense pulses and show a coherent vortex for a longer time period. However, none of these simulations with a cyclone

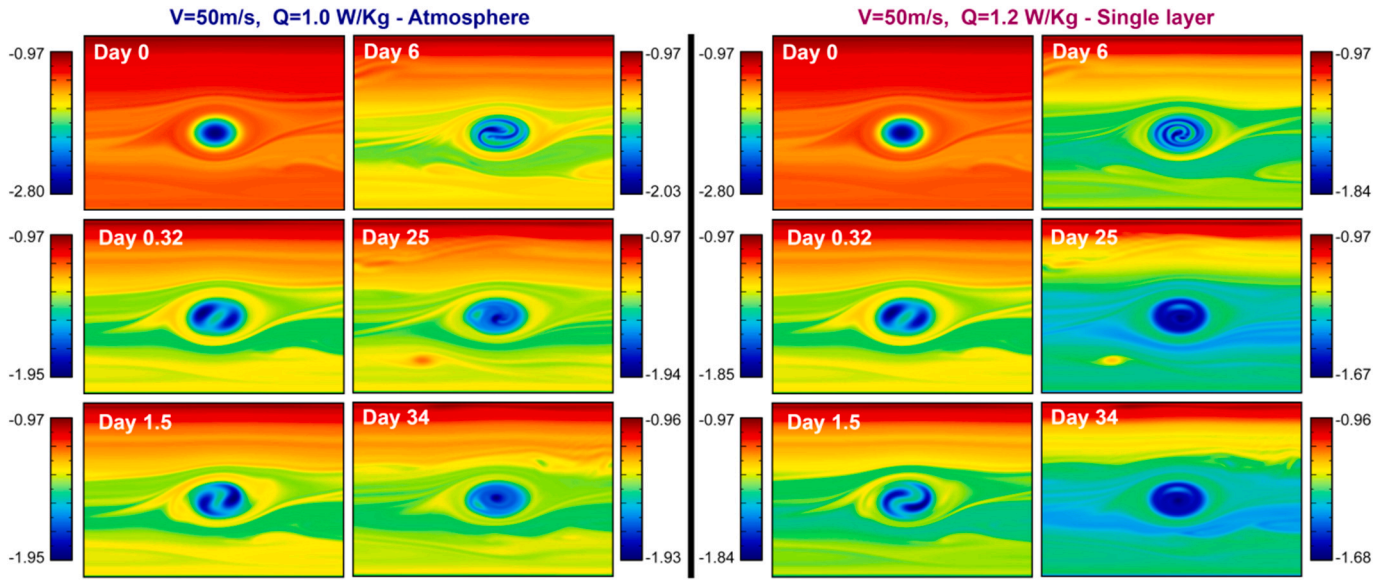

Fig. 7. Detailed evolution of the vortex-storm system at cloud level in two simulations with heat pulses introduced differently. Panels show potential vorticity q in units of 10^{-6} m^2Ks^{-1} kg^{-1} at a mean pressure of 620 mbar. The domain represented is 10° in latitude and 15° in longitude. Left panels: Vortex with a tangential velocity of 50 ms^{-1} and a heat pulse of 1.0 Wkg^{-1} active over 0.25 days with a size parameter $a = 0.5°$ and introduced in all layers except the abyss. Right panels: Same vortex but now perturbed with a convective pulse active for the same time and with the same size but with an intensity of 1.2 Wkg^{-1} and introduced only in the interface between the layers at 620 and 1700 mbar. The spatial resolution of both simulations is 0.04°.

with an initial weak circulation reproduces the short-term morphology observed in Clyde's Spot.

The lower three rows of Fig. 8 show results for stronger vortices with initial velocity fields with tangential velocities of 50 ms^{-1}. Convective pulses of $\dot{Q}_0 \sim 1.0$ Wkg^{-1} reproduce reasonably well the initial phases of Clyde's Spot (Fig. 1b) as shown in Figs. 5A and B. However, these vortices become quite homogenous after 10 and 25 days, and depart from the complex structure and long-term phenomenology observed in Clyde's Spot (Hueso et al., 2022). More intense convective pulses of $\dot{Q}_0$=2.0 Wkg^{-1} and $\dot{Q}_0$=3.0 Wkg^{-1} are needed to form the complex structures observed in Clyde's Spot months and a year after the onset of the storm (Fig. 8d), although in these simulations, similar complex structures are formed in a matter of a few days. This suggests that the complex long-term phenomenology observed requires sustained convection over larger time-scales injecting twice or three times the initial energy released during the initial convective pulse but at a much smaller pace.

If we compare the results from the two different convective schemes we find that simulations with energy introduced in all vertical layers (columns b_1 and b_2) are more similar to the observations than the simulations where energy is only introduced in the interface between 620 and 1700 mbar (columns c_1 and c_2 in Fig. 8). Fig. 9 shows a larger section of two of the simulations shown in Fig. 8 and focuses on the differences from using one convective scheme or other. The upper panel in Fig. 9 shows the evolution of the cyclone after the short convective pulse introduced in all model interfaces ten days after convection is switched off. The simulation produces a folded filamentary feature that reminds the morphology of Clyde's Spot months after the storm. The same structure is not obtained when introducing convective energy only in the limited region between 620 and 1700 mbar, but more intense pulses, or additional energy introduced in the model might be needed to reproduce those later stages of the observations.

In addition, simulations of very intense vortices ($V = 75$ ms^{-1}) not shown in Fig. 8 resulted in fast homogenization of the vortex, and we conclude that these strong vortices cannot be perturbed with a strength large enough to break the confinement produced by the vortex circulation and are disregarded as possible cases for the development of the convective storm.

4. Convective storms in the SSTB and the SEB

A similar convective storm inside a cyclone was observed by Voyager 2 in the SSTB (Smith et al., 1979b), and an image of its first stages is shown in Fig. 1d. The storm developed a double-lobed structure very quickly and similarly to the STB storms in 2020 and 2021. It later evolved in a few days into a complex turbulent area known as a Folded Filamentary Region (FFR) remaining as a stable FFR over the rest of the Voyager 2 flyby. Further images of this storm are shown in Hueso et al. (2022). A very different storm was observed by Voyager 1 in the SEB a few months earlier. This was a storm that originated in a small cyclone and developed actively over 7 days, quickly and largely exceeding the size of the cyclone where it developed and strongly interacting with the zonal winds over a longer time-scale (Fig. 1f and g). The storm never exhibited the double-lobed structure observed in Clyde's Spot or the SSTB storm. Hueso et al. (2002) present a study of this storm including evaluations of the possible energy required to drive such a large convective system. Several similar storms were observed in the SEB months later by Voyager 2 (Smith et al., 1979a, 1979b). Together they represented a spectacular set of storms that did not affect the whole SEB as in classical SEB Disturbances (Sánchez-Lavega and Gómez, 1996; Fletcher et al., 2017). Here we simulate these storms in the SSTB and SEB using the same approach as for the storms in the STB. The ranges of values tested to simulate these storms are summarized in Table 3 and Table 4. For simplicity, we did not consider vertical wind shears that could be associated to the latitudes of any of these two storms.

4.1. Simulations of the convective storm in the SSTB

For the storm in the SSTB we considered an initial cyclone with the size it had before the convective eruption (semi-major axis 4.05° and semi-minor axis 1.7°, making this cyclone significantly larger than those in the STB simulated above), and we assumed a cyclonic tangential velocity of 30 ms^{-1}. This value comes from the analysis of Voyager images in Hueso et al. (2022). We also used the same model atmosphere initialization and vertical extent of the vortex as in the previous sections, except for two obvious differences: initializing the storm at its observed latitude (−38.8° planetographic), and using the environment winds

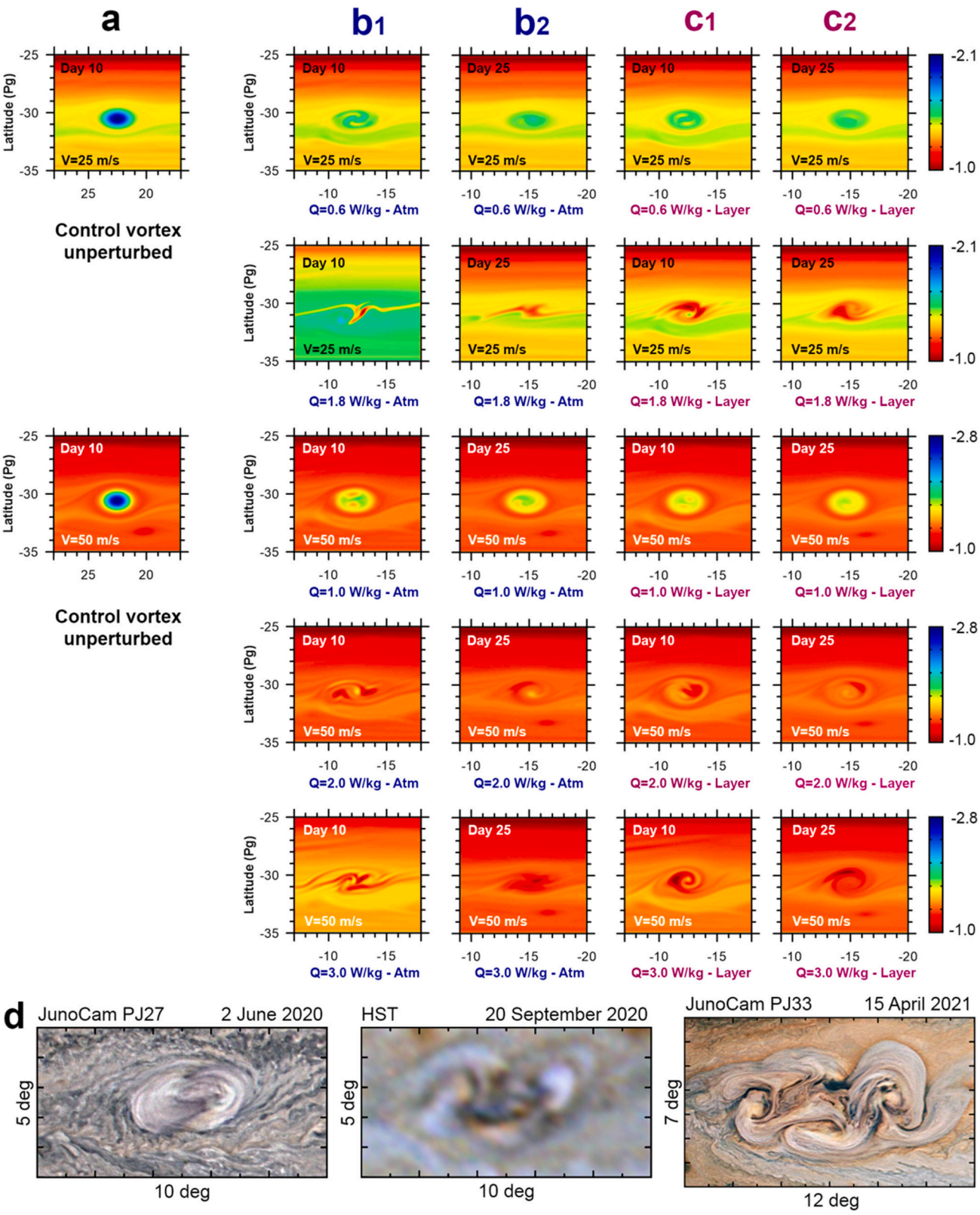

Fig. 8. Simulations for a variety of vortex tangential velocities and intensity of the convective pulse. Maps represent subsections of the potential vorticity field q in units of 10^{-6} m^2Ks^{-1} kg^{-1} from the isentrope at an average pressure of 620 mbar and centered over the vortex. The upper two rows show results for cyclones with initial tangential velocities of 25 ms^{-1}. The next three rows show results for cyclones with initial tangential velocities of 50 ms^{-1}. Column (a) shows the initial cyclones. Columns (b_1) and (b_2) show results for simulations with the convective pulse vertically distributed over the atmosphere. Columns (c_1) and (c_2) show results for simulations with the convective pulse concentrated on a single interface between the isentropes from 620 to 1700 mbar. Times represented are 10 and 25 days after the short convective pulse. Details are given in each subpanel. All simulations were computed with a spatial resolution of 0.08°. Row (d) shows JunoCam and HST observations of the evolution of Clyde's Spot and its remnant at different time instants, from left to right 2.5, 112 and 320 days after the onset of the convective storm.

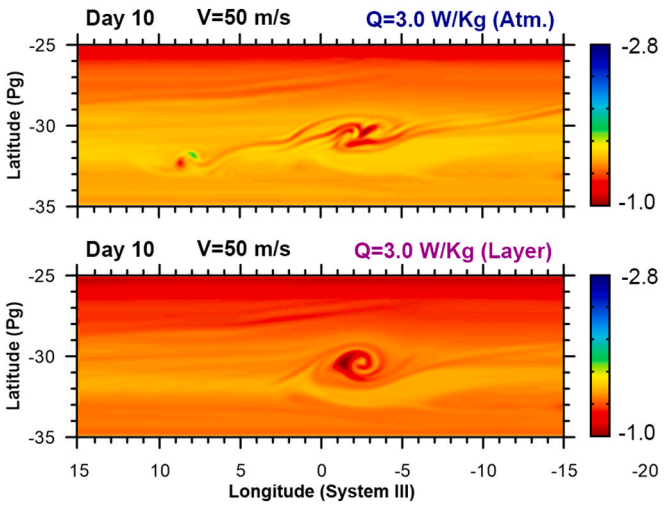

Fig. 9. Output of two identical simulations except for the scheme used to introduce the convective pulse. The top panel shows results when the convective pulse is introduced affecting the full vertical structure of the vortex, and the bottom panel when energy is only introduced in the region between the isentropes from 620 to 1700 mbar. Maps represent the potential vorticity field (q in units of 10^{-6} m^2Ks^{-1} kg^{-1}) from the isentrope at an average pressure of 620 mbar and the simulations were computed with a spatial resolution of 0.08°.

retrieved from the analysis of Voyager data (Limaye, 1986). Also, the larger size of the initial cyclone let us use a spatial resolution of 0.08° per grid point.

We found that convective pulses of 0.3–0.5 Wkg^{-1}, sizes determined from the compact clouds observed in the Voyager sequence with a = 0.8° and b = 0.65°, and durations of 0.5–1.0 days result in a disturbed cyclone that develops into an FFR-like feature rapidly in a few days. Fig. 10 presents some of these simulations using both types of convective pulses, either affecting the whole vertical structure of the vortex, or only the interface between the isentropes with averaged pressures of 620 and 1700 mbar. In this case, we did not attempt to run a full exploration of the space of parameters, since our initial simulations were successful in reproducing the initial stages of the storm's evolution, and there is less observational information for this storm. The overall transformation of the convective cyclone into a FFR is better reproduced in simulations where the full vertical structure of the vortex is affected by the convective pulse.

The key differences in this storm compared with the 2020–2021 STB storms are the larger size of the cyclone and the weaker intensity of its outermost tangential velocity. This results in the possibility in the simulations of larger convective pulses that are active for a longer period of time but with lower intensities. Thus, although the intensity of convection is smaller, the total energy injected in this cyclonic storm system is larger than the energy required to reproduce the morphology of Clyde's Spot. The simulations disturb the cyclone and turn it into a turbulent cyclonic region that reorganizes similarly to an FFR in a time-scale of a few days, similarly to the observations and very differently to what was observed for Clyde's Spot.

4.2. Simulations of the convective storm in the SEB

The large storm in the SEB observed by Voyager 1 in 1979 was very different and particularly difficult to simulate. We used the same model atmosphere as in the rest of this manuscript, except that the storm was launched at 16° S latitude and we used the Voyager winds (Fig. 2). We tested different values of the intensity, size and time duration of the convective pulse. We did not introduce an initial cyclone as in the simulations presented for the storms above. In this case, the very small size of the initial cyclone observed in Voyager images and the fast increase of the storm beyond the initial cyclone in a few hours made this a reasonable hypothesis. We also made simulations with the two convective schemes. Among the combinations of the range of parameters tested in this work to reproduce this SEB storm, the second convective scheme in which energy is deposited only in the interface between two isentropes produced results much closer to the morphology observed than the first convective scheme.

Our most successful simulation of the evolution of the morphology of this storm is shown in Fig. 11, which compares snapshots of the storm with the simulation. This simulation used a convective pulse with the same size as the one used for Clyde's Spot, $a = b = 0.5°$, had a power release of 0.5 Wkg^{-1} and was kept active for 7 days. This time duration was extracted from the analysis of the divergence of clouds presented in Hueso et al. (2002). The spatial resolution of this simulation was 0.08°/pix. The simulation successfully reproduces the overall shape of the cloud field observed by Voyager. Note the anticyclonic motions of the central system in the simulation and its interaction with the cyclonic jet. Several other simulations were attempted, but only simulations with roughly an equivalent amount of energy, and very close to the values of the parameters of the convective pulse described above, were able to match the morphologies of the clouds observed in the Voyager images.

The large size of this storm was possible only through sustained convection instead of the limited convective eruptions observed in Clyde's Spot and the other storms inside closed cyclones here simulated.

5. Discussion

5.1. Analysis of the simulations

Clyde's Spot (Fig. 1a and b), the equivalent 2021 STB storm (Fig. 1c) and the 1979 storm in the SSTB (Fig. 1d), are similar in some aspects and different in others to the 2018 storm in the STB Ghost (Fig. 1e) reported in Iñurrigarro et al. (2020). These convective storms occurred inside closed cyclones of different sizes and tangential velocities and largely disturbed the full cyclone in which they developed. In all cases, the consequences of the convective outbreaks were confined to the interior of the cyclone that later evolved over months in a complex way. The 2018 STB storm occurred inside a large elongated cyclone with a velocity in the outer parts of the cyclone of 50 to 80 ms^{-1} and displayed convection over a time-scale of 2–4 days. Its later evolution seems to suggest a break-up of the cyclone in two sides, which required an intense energetic perturbation because of the large external tangential velocity measured from analysis of Junocam images. The convective eruption in the SSTB in 1979 was an intermediate case in terms of the size of the cyclonic system and also the duration of convection, here modeled with a convective pulse of one day. The convective outbreaks in Clyde's Spot and in the 2021 STB cyclone occurred in smaller cyclones and were active for the shortest periods, being modeled here with convective pulses of 0.25 days. The convective eruption in the SEB (Fig. 1f and g) was very different. While it also started inside a small cyclone, it quickly grew to a very large size and stayed active for 7 days from the analysis of Voyager observations in Hueso et al. (2002).

Observations of the storms in the STB and the SSTB discussed in Hueso et al. (2022) show that the cyclone-storm system acquired a double-side morphology in a time-scale of 2 days that rotated and reorganized in turbulent patterns during tens of days (in the SSTB) or several months (in the STB) to form in both cases a complex FFR. The double-side morphology and the time-scale for its development are well reproduced by our nominal numerical simulations of the potential vorticity field with the EPIC model and suggest the short convective pulses modeled. This double-side feature is also absent in the evolution of storms in the SEB.

In the 2018 storm in the STB Ghost discussed in Iñurrigarro et al. (2020), patterns of bright clouds were formed and circulated inside the elongated cyclone producing a complex phenomenology that was very different to the cases studied here. Three consecutive convective pulses

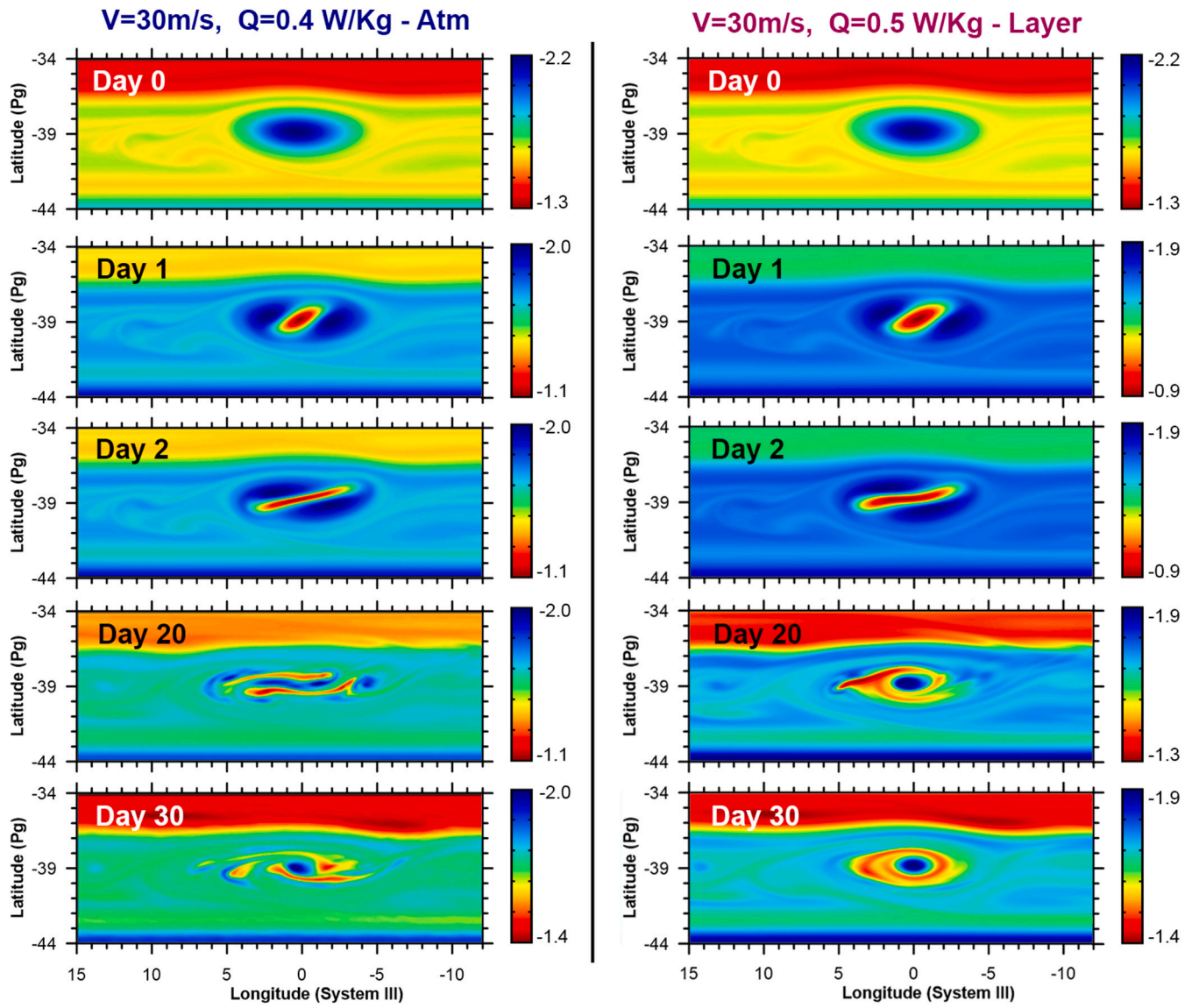

Fig. 10. Sections of our EPIC simulations of the Voyager 2 SSTB storm showing potential vorticity in units of 10^{-6} m^2Ks^{-1} kg^{-1}. Left and right panels show the evolution of two different simulations with a convective pulse of 0.4 Wkg^{-1} introduced in all the vertical structure of the vortex (left) and with 0.5 Wkg^{-1} only affecting the region between the isentropes at 620 and 1700 mbar (right).

were observed, and the size of the STB Ghost was large enough to produce a recirculation of the cloud material generated in the convective outbreak (Fig. 1e). Part of the initial bright features transformed in dark patches quickly, and a later stage of turbulence inside the cyclone was observed for a long period of time. These dark patches and turbulence patterns were also observed in Clyde's Spot and the 2021 STB storm. Numerical simulations of the 2018 storm in the STB Ghost with EPIC in Iñurrigarro et al. (2020) similar to those presented here used three convective pulses vertically extended over the atmosphere and with intensities of 0.4–0.7 Wkg^{-1}, but those pulses were long with durations of 2–4 days. Compared to the simulations presented here for Clyde's Spot, the convective pulses in Iñurrigarro et al. (2020) were activated over larger areas and with longer time durations producing a much larger convective event. In Clyde's Spot, numerical simulations suggest that a single, short and intense convective pulse of 1.0–1.2 Wkg^{-1} (either introduced distributed over the vertical structure of the vortex or only in a single interface) is able to reproduce the observed phenomenology. However, the combination of size, intensity and duration results in a much lower release of energy in the small storms in the small cyclones of the STB in 2020 and 2021 when compared with the larger convective outbreaks in the STB Ghost in 2018.

The 1979 SSTB storm occurred on a different latitude in a weaker cyclone with a probable tangential velocity of 30 ms^{-1}, but with an intermediate size from the 2018 STB Ghost and the 2020–2021 STB storms. This storm can be simulated with a convective pulse of 0.4–0.5 Wkg^{-1} (either introduced distributed over the vertical structure of the vortex or only in a single interface) acting over a time-scale of one day over a larger area than in the 2020–2021 STB storms.

The storm in the SEB here simulated started in a cyclone of unknown circulation, and its morphology can be reproduced with a relatively weak convective pulse of 0.5 Wkg^{-1} active for a long period of 7 days.

In each of the storms studied in this work the total energy injected in the atmosphere in each simulation can be estimated as:

$$E = 2Q_0 \pi ab \frac{P_{\max} - P_{\min}}{g_{eff}} \Delta t \tag{5}$$

Here Δt is the total time the storm is active, πab is the area of the convective pulse, the factor 2 is an approximate correction to take into account the Gaussian shape of the convective pulse, g_{eff} is the effective gravity acceleration at the latitude of the storm taking into account

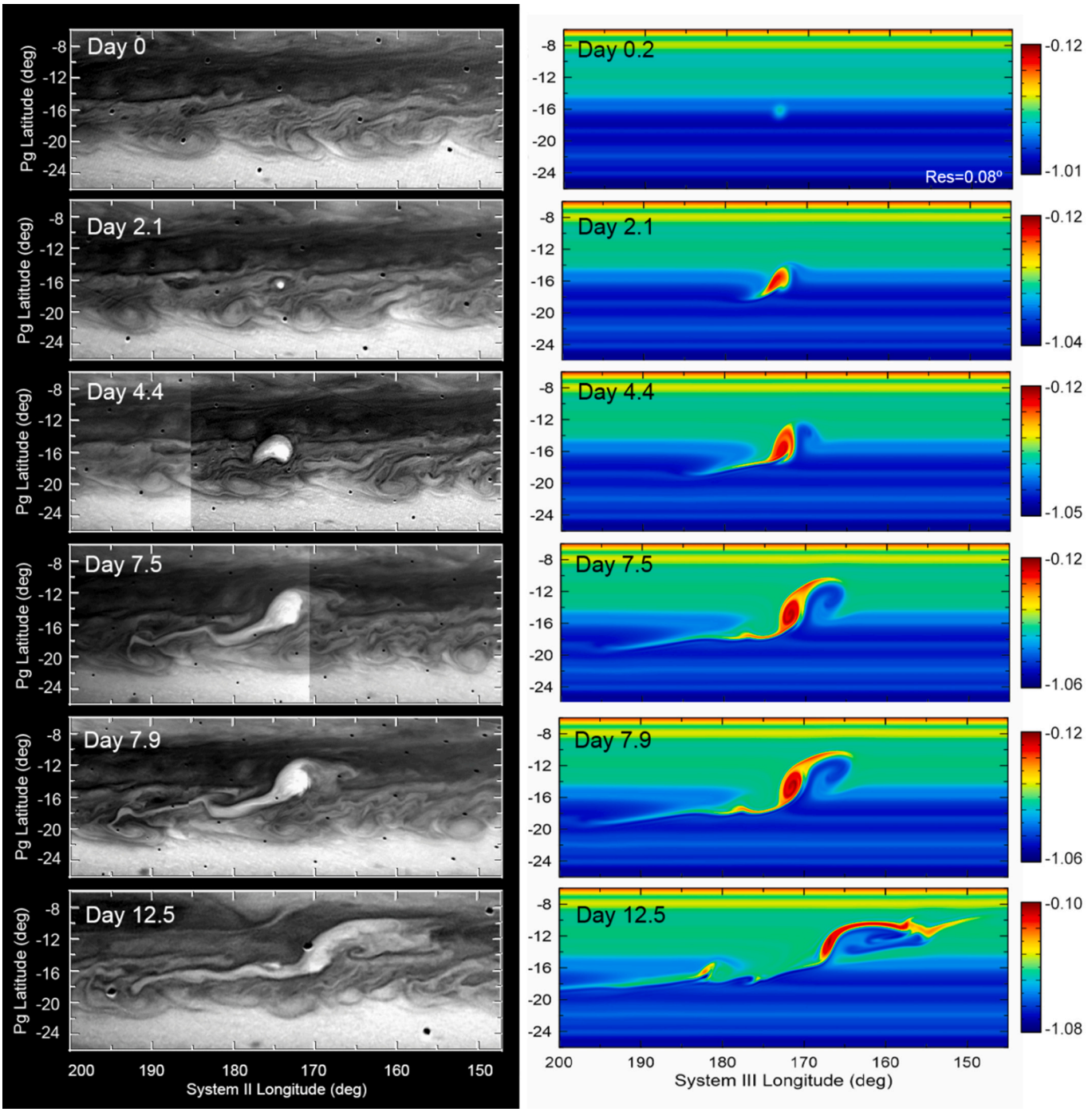

Fig. 11. A large storm in Jupiter's SEB. Left panels: Maps of a large storm in Jupiter's SEB observed by Voyager 1 from Hueso et al. (2002). Right panels: Maps of an EPIC simulations showing potential vorticity in units of 10^{-6} m^2Ks^{-1} kg^{-1} at the isentrope with mean pressure of 620 mbar.

Jupiter's rotation period, and P_{max} and P_{min} are the maximum and minimum pressure of the convective pulse. Depending on which convective scheme is used, the values of P_{max} and P_{min} are 7 bar and 30 mbar when introducing a vertically extended pulse, or 1700 and 620 mbar when introducing energy only in the interface closer to the observable level. It is important to note that although both types of convective pulses result in very different total energies, the amount of energy introduced at the levels where moist convection deposits energy is similar in both set of simulations.

If we compare simulations with the same value of $\dot{Q}_0$ but introduced in a single model interface instead of vertically through the atmosphere, then we find total energies that are roughly 6.4 times smaller. Since these simulations are closer to what we expect from a convective storm in which energy is transported to the upper troposphere from the deep reservoir of water, we will use these values as a very rough estimate of the energy implied by our simulations. However, since there are clear uncertainties in how much of the energy we introduce in the model can be considered as representative of convection, a relative scale of energy between the different simulations might be more appropriate than an absolute scale.

Table 5 presents the estimated values of the total energy deposited in the simulations following eq. (5) and considering values of $P_{min} = 620$ mbar and $P_{max} = 1700$ mbar. For the energy values of the 2018 storm in the STB Ghost we used energy values obtained by Iñurrigarro et al.

Table 5
Heating amplitudes and energies involved by the simulations that reproduce each storm.

Storm	$\dot{Q}_0$ (Wkg^{-1})	a (deg)	b (deg)	Δt (days)	E (J)
1979 SEB	0.5	0.5	0.5	7	3.8×10^{21}
1979 SSTB	0.5	0.80	0.65	1	0.8×10^{21}
2018 STB	0.4–0.7 (3 pulses)	(different sizes and durations for the three pulses but active convection from 2 to 4 days)			4.6×10^{21}
2020 STB	1.2	0.5	0.5	0.25	0.25×10^{21}
2021 STB	1.2	0.5	0.5	0.25	0.25×10^{21}

(2020), who considered vertically extended convective pulses. Thus, values in Table 5 are corrected from the 6.4 correction factor described above.

5.2. Local water abundance in the 2020 and 2021 STB storms

The energy released in the 2020 and 2021 STB storms can be compared with the amount of water and ammonia condensation that would be needed to release that heat. The energy released per unit of mass is $\dot{Q}_0$ multiplied by the time the storm is active. Dividing this number by the latent heat of water, we can estimate the amount of water per unit of mass implied. Using a water latent heat of 2834 J/g and the data in Table 5, we obtain 9 g of water per kg of atmosphere in the two storms in the STB. Note that a similar calculation for the other storms in Table 5 is not immediate, as those storms are active over long time-scales with significant divergence in the upper clouds. Those storms are sustained convective phenomena feeding of volatiles from their environment inside the large cyclone where they arise complicating the interpretation of a similar calculation. However, in the short convective pulses associated to the 2020 and 2021 STB storms, in which convection is local and affects the whole cyclone over the same time-scale, the updraft cannot feed from its environment. Thus, the amount of water mass per unit of atmospheric mass can be used as a rough estimation of the amount of water that would be needed to power convection. The value obtained for the 2020 and 2021 STB storms, 9 g of water per kilogram of atmosphere, is equivalent to a molar abundance of 1.14×10^{-3}, or a local water abundance of 1.2 times solar (with the protosolar values from Asplund et al. (2009) taken as the solar values).

The same amount of energy could be released by ammonia only by condensing an unreasonably large amount of ammonia. Considering an ammonia latent heat of 1836 J/g, about 14 g of ammonia per kg of atmosphere should condense in these storms, implying a local ammonia abundance of 14 times solar, which is ~5 times larger than the deep value measured by the Juno's MWR experiment (Li et al., 2017). If both water and ammonia contribute to the energy budget of a storm like Clyde's Spot, and ammonia is limited to a value of 2.8 times solar abundance, as implied by Juno's measurements, then a 1.0 solar abundance of water is required to form storms like the two events observed in 2020 and 2021.

Since condensables can be distributed differently on different Jovian locations, this is only a reasonable conjecture on the local value of water at the time these storms occurred. Furthermore, these estimates are only a lower limit of the abundance of water, since it has been assumed that all water in the location of the storms is used in the storms.

5.3. Relative scales of energies of convective storms

For a sense of scale the 0.25×10^{21} J attributed to Clyde's Spot are equivalent to 3.4% of the total internal energy flux of 5.5 Wm^{-2} over the whole planet, ~3.4×10^{17} W, which could be transported by 30 similar storms if moist convection was the predominant factor in transporting this internal heat. If the energy was calculated heating the atmosphere from the water condensation level to the upper troposphere, the energy associated to this storm would increase to 22% of the total internal energy flux. However, we note that convective storms such as those described in this paper are indeed rare. The three consecutive events in the STB from 2018 to 2021 shown in Table 5 occurred in a period of 4 years. However, we do not have a survey of convective storms in Jupiter complete enough to quantify the amount of comparable storms that could occur in Jupiter. For instance, Hueso et al. (2022) discuss the possibility that one additional cyclone in the STB could have developed a not observed convective storm in 2019 from its changes in morphology from 2019 to 2020. From the existing survey of observations in Jupiter including HST and amateur images, it is clear that there are not enough strong convective storms active over a year in Jupiter to transport its internal heat. Instead, weaker moist convection, not strong enough to show intense activity at the upper clouds, but producing deep lightning, seem to occur more widely over the planet (Little et al., 1999; Brown et al., 2018). Intriguingly, observations of lightning from Juno show that lightning activity was particularly infrequent at the STB latitude at least in 2016–2017 (Brown et al., 2018).

While the absolute numbers associated to energy in Table 5 represent very rough estimates of the total energy needed to produce the phenomenology observed in each storm, a relative comparison of the energy required to reproduce the observed morphologies of the different storms can be established.

The total energy released in the 2018 STB Ghost storm was 18 times larger than the energy released in the initial phase of Clyde's Spot. This is larger than the differences in area of the bright clouds observed in methane band images 2–3 days after the outburst in both storms (Fig. 1a and Fig. 1e). The large energy of the convective eruptions in the STB Ghost corresponds to simulations in Iñurrigarro et al. (2020) that broke the STB Ghost. This was an observational effect that the simulations reproduced. Those simulations considered an outer tangential velocity of the STB Ghost of 80 ms^{-1} based on wind measurements from Junocam images, thus, requiring a strong energy input. Thus, if the winds around the STB Ghost were smaller a lower amount of convective energy would have also resulted in a similar result.

The SEB storm observed by Voyager 1 in 1979 had an energy scale 15 times larger than Clyde's Spot. Note that, although this was a large-scale storm it was not a convective storm leading to a planetary-scale disturbance as it occurs in disturbances of the SEB described by Sánchez-Lavega and Gómez (1996) and Fletcher et al. (2017). The value of energy estimated here for this particular storm in the SEB, 3.8×10^{21} J, compares reasonably well with the 6.0×10^{21} J value estimated in Hueso et al. (2002) for the same event. That value was calculated following the scheme presented by Banfield et al. (1998) for storms near the GRS. Those estimations come from the size of the convective clouds and the expected thermal energy released by water moist convection heating the troposphere at the visible cloud level by a given ΔT over a scale height (the calculation in Hueso et al. (2002) for the storm in the SEB considered $\Delta T = 5$ K from powerful water moist convection). The conclusion from Hueso et al. (2002) was that this energy release would require a deep water solar abundance of 2 times solar. The lower energy estimate here would scale down requiring only 1.2 times water solar abundance. The 3.8–6.0 $\times 10^{21}$ J energy range would also translate into a power release of 6.3–9.9 $\times 10^{15}$ W, comparable to the convective power of 5×10^{15} W obtained by Gierasch et al. (2000) in an analysis of convective storms near the GRS observed by Galileo. That power evaluation followed essentially the same arguments as in Banfield et al. (1998) and was based on the size of the active storm with similar hypothesis on the amount of heating in the troposphere.

The storm observed in 1979 by Voyager 2 in the SSTB was intermediate in strength, releasing 3 times more energy than Clyde's Spot and the 2021 STB storm. This enhanced energy compared with Clyde's Spot could help to explain the short time evolution of a few days between the storm's onset and the formation of a fully formed FFR. In fact, simulations of Clyde's Spot with convective pulses of 3.0 Wkg^{-1} (Fig. 9) and total energy releases of three times the nominal simulations that

reproduce the original outburst reproduced a fast formation of a FFR. We remind that a FFR was indeed formed from Clyde's Spot through a slow evolution of several months in which bright filaments were occasionally observed. This supports the idea of sustained weak convection in Clyde's Spot over a long time scale after the original explosive outburst.

5.4. Availability of condensables in different convective storms

Previous attempts to understand convective storms in Jupiter have focused in the large-scale perturbations of certain bands, where convection starts suddenly from a small location and grows over time-scales of days interacting with the zonal winds (Sánchez-Lavega et al., 2008; Fletcher et al., 2017). For instance, the SEB simulation presented in Fig. 11 considered a convective pulse of 7 days consistent with the expanding rate of clouds. The storms originated in small cyclones like Clyde's Spot operate in a very different way. Convection in these closed cyclones stops in hours to days and the environment vortex circulation confines the clouds produced in the convective eruption. The 2018 storms in the STB Ghost were an intermediate case in which three convective storms originated inside a large cyclone and were active during 2–4 days. The storm in the SSTB is also an intermediate case in size, energy and duration between the storms in the STB Ghost and Clyde's Spot.

We suggest that the local availability of condensables is the element that makes these convective storms different. A vertically coherent cyclone isolates the local atmosphere from its environment and limits the capacity of the storm to feed on condensables from their environment outside the cyclone. Convective storms formed outside a vortex can acquire condensables from a larger area evolving over much longer time-scales. The exception to this are the outbreaks in the SEB, where convective sources start from small cyclonic features that are quickly broken allowing the storm to gather condensables from their environment. Convection in small but intense vortices like the cyclones in the STB is limited in size and energy. Convective storms in larger cyclones like those of the SSTB can feed from condensables over a larger area and develop into more energetic events. Convection in much larger cyclones like the 2018 storms in the STB Ghost have a larger potential supply of condensables and are able to grow over a longer time, releasing more energy and developing more intense phenomena. While the short-term evolution of Clyde's Spot can be explained by a short and intense release of energy, its long-term evolution discussed in Hueso et al. (2022), included the slow growth and formation of a FFR structure. This required additional energy, which from the simulations here presented was at least three times as intense as the initial outburst but sustained over a large time period. The strong circulation at the visible cloud level around Clyde's Spot with tangential velocities of 50 ms^{-1} observed in September 2020, months after the storm developed, confined the vortex efficiently. It is unlikely that ammonia convection could release the extra energy required to drive that dynamics. We speculate that slow and sustained water moist convection drove the transformation of Clyde's Spot into its FFR stage and that the circulation of the vortex at the water condensation level after the initial outbreak could be weaker than at cloud level allowing the introduction of water inside the cyclone to feed sustained convection.

6. Summary and conclusions

In a series of 2 papers we have presented a thorough analysis of the convective storm known as Clyde's Spot and similar storms occurring in closed cyclones in Jupiter's atmosphere. In Hueso et al. (2022) we presented the observational analysis, and here we have presented results of numerical simulations of these storms using the EPIC numerical model and the comparison with results for the convective storm in Jupiter's STB Ghost that occurred in 2018 and analyzed in Iñurrigarro et al. (2020). We also provide an additional comparison with one large storm in the SEB that was studied in detail by Hueso et al. (2002) from Voyager images, and that was one of several convective eruptions that did not develop into a full SEB Disturbance. Here is a list of our main conclusions from these numerical simulations and comparisons.

- Clyde's Spot, a short-lived convective storm that started inside a closed cyclone in 2020, and a similar storm observed in the STB in 2021, originated in cyclones that were the result of the merger of smaller cyclones. Numerical simulations of small cyclones in the STB show that cyclones merge naturally forming cyclones of larger area without resulting in significant changes in their outermost velocities. The simulated merger occurs without producing additional activity or releasing turbulence to the environment. The merged cyclone has a similar vertical structure to the original cyclones and only a limited capacity to deepen into the lower atmosphere. It is unclear from our simulations if the vortex merger is related with the development of moist convection months after the merge. Our simulations do not have the capacity to reproduce the possible interactions of the vortex where Clyde's Spot originated with the GRS.

- A convective storm developing in the center of a closed cyclone develops anticyclonic vorticity forming naturally a double side-lobed structure that rotates cyclonically. This double-side structure is formed in one to a few days according to observations of the 1979 storm in the SSTB and the formation of Clyde's Spot in the STB in 2020 and a similar storm in the STB in 2021. Compared to other simulations, the formation of this double-lobed structure requires an intense and short convective pulse. If the convective pulse is too intense or too long, the double-lobed structure does not develop and the storm can overcome the size of the initial cyclone as in the storms in the SEB.
- The outcome of the evolution of storms in cyclones depends on the intensity of the cyclonic circulation and the energy released in the storm. In most of the storms here simulated, the vortex circulation was strong enough to contain the material spread from the convective outbursts. This is different to what happens in perturbations in the SEB where convective outbursts start in small cyclonic regions but break those completely. The mechanism by which these storms in closed cyclones erupt remains to be explored and requires a dynamical model of cyclones with condensables.
- Convective storms such as the events in the STB from 2018 to 2021 are rare. While each one of them has a strong energetic impact equivalent to a fraction of Jupiter's total internal heat (~3.4% according to our best estimation), more widely distributed, and less intense storms operating regularly under Jupiter's clouds, should have a larger total contribution to the total transport of energy in Jupiter's atmosphere.
- For the convective storms inside closed cyclones here studied, the amount of energy released was very different. The 2018 storm in the STB Ghost was ~18 times more energetic than Clyde's Spot, and the storm in 1979 in the SSTB was ~3 times more energetic than Clyde's Spot. We estimate that large storms in the SEB as the one discussed in Hueso et al. (2002) release about ~15 times more energy than Clyde's Spot. Full disturbances of the SEB should release an amount of energy at least ten times larger, as the 1979 singular storm observed by Voyager 1 was followed by several similar events observed by Voyager 2 months later. The apparent larger amount of energy computed for the storm in the STB Ghost compared with the storm in the SEB is a consequence of the intense tangential velocity of 80 ms^{-1} in the STB Ghost where the storm originated. The energy estimated in the storm in the STB Ghost could have been smaller if the tangential velocity of the STB Ghost was overestimated.
- For the short convective pulses associated to the 2020 and 2021 STB storms, EPIC simulations suggest a local water abundance of at least 1.0–1.2 times solar in the location of these storms, with the lower number implying a substantial role of ammonia condensation when

forming the storms, and the larger number implying only water. The same calculation cannot be done for the other storms analyzed in this work, since their longer times of activity are consistent with sustained feeding of volatiles from their close environment inside the large cyclone.

- The differences in energy of the convective systems here studied can be related with the differences in the size of the cyclones where the storms developed. The 2018 STB Ghost was ~15 times larger in area than the cyclone where Clyde's Spot originated, and the storm in 1979 in the SSTB originated in a cyclone that was ~4 times larger than Clyde's Spot cyclone. We propose that the local availability of condensables limits the energetic development of storms created in cyclones. If the storms are powered by water moist convection, then the vortex extends at least to the water cloud base limiting the deep feeding region of the storm. Convective systems like the SEB storm where the storm expands to larger sizes than their cyclonic source have access to larger areas and can feed from condensables supplied for a longer period of time.
- While Clyde's Spot and the similar convective storm in 2021 were the storms systems releasing the smallest energies in the set of convective systems here studied, they were also those releasing the highest power. Our simulations suggest a fast and short-lived power release of 1.2 Wkg^{-1} in Clyde's Spot. This contrasts with the long convective pulse of 0.5 Wkg^{-1} required to simulate the SEB storm observed by Voyager 1. Previous analysis of that storm suggested deep water abundances of 2.0 times solar, which from the calculations here explored could be lowered to 1.2 times solar abundance. This is equivalent to the minimum local water abundance of 1.0–1.2 times solar calculated for Clyde's Spot.
- The short-term evolution of Clyde's Spot can be explained by a short and intense release of energy. Its long-term evolution, which included the slow growth and formation of a FFR structure, required additional energy, which was at least three times as intense as the initial outburst. We speculate that the intense circulation of Clyde's Spot at cloud level could be smaller at the water condensation level allowing the introduction of additional condensables inside the vortex at its base, enabling its long-term slow evolution into a large FFR.

The convective phenomena here examined are generally short-lived and affect a limited longitudinal range, not developing into planetary-scale disturbances like those that can occur at the SEB (Sánchez-Lavega and Gómez, 1996; Fletcher et al., 2017), or the ones that occur in the North Temperate Belt (Sánchez-Lavega et al., 2008, 2017). During those events, the plumes that form the disturbances remain active for a timescale of over a month with various outbreaks triggering sequentially at different longitudes and disturbing globally the entire latitudinal band. Their larger scale and capability to remain active for such long periods will require specific simulations that will help to establish a full scale of energies associated to the variety of convective events in Jupiter. The smaller but intense convective storms here simulated open tantalizing questions about the role of moist convection of different scales and frequencies in supporting the transport of Jupiter's internal heat to the upper troposphere. An in-depth exploration of the frequency and activity of large-scale (NTBD or SEBD-like events), intermediate and short-lived storms (such as those in the STB), and small convective storms (such as those implied from observations of lightning) might be needed to assess the role of moist convection in the global transport of Jupiter's internal heat.

Data availability

The EPIC model can be downloaded from the Atmospheres Node of the Planetary Data Service at: https://atmos.nmsu.edu/data_and_services/software/epic/epic.htm. Observations discussed in this paper are available as documented on Hueso et al. (2022). Additional Voyager 1 observations are documented on Hueso et al. (2002) and are accessible through The PDS Ring-Moon Systems Node's OPUS search service at https://opus.pds-rings.seti.org/opus/.

Declaration of Competing Interest

None.

Acknowledgements

We are very grateful to Clyde R. Foster, John H. Rogers and G. S. Orton for discussions on the complex phenomenology around Clyde's Spot. We are also grateful to two anonymous reviewers that provided detailed and constructive comments that improved the contents of this paper. This work has been supported by Grant PID2019-109467GB-I00 funded by MCIN/AEI/10.13039/501100011033/ and by Grupos Gobierno Vasco IT1366-19. PI acknowledges a PhD scholarship from Gobierno Vasco.

References

Asplund, M., Grevesse, N., Sauval, A.J., Scott, P., 2009. The Chemical Composition of the Sun. Annu. Rev. Astron. Astrophys. 47 (1), 481–522. https://doi.org/10.1146/annurev.astro.46.060407.145222.

Banfield, D., Gierasch, P.J., Bell, M., Ustinov, E., Ingersoll, A.P., Vasavada,, A.R., West, R. A., Belton, M.J.S., 1998. Jupiter's cloud structure from Galileo imaging data. Icarus 135, 230–250. https://doi.org/10.1006/icar.1998.5985.

Bjoraker, G.L., Wong, M.H., de Pater, I., Hewagama, T., Ádámkovics, M., Orton, G.S., 2018. The gas composition and deep cloud structure of Jupiter's Great Red Spot. Astron. J. 156, 101, 15pp. https://doi.org/10.3847/1538-3881/aad186.

Brown, S., Janssen, M., Adumitroaie, V., Atreya, S., Bolton, S., Gulkis, S., Ingersoll, A., Levin, S., Li, C., Li, L., Lunine, J., Misra, S., Orton, G., Steffes, P., Tabataba-Vakili, F., Kolmasová, I., Imai, M., Santolík, O., Kurth, W., Hospodarsky, G., Gurnett, D., Connerney, J., 2018. Prevalent lightning sferics at 600 megahertz near Jupiter's poles. Nature 558, 87–90. https://doi.org/10.1038/s41586-018-0156-5.

Dowling, T.E., Gierasch, P.J., 1989. Cyclones and moist convection on Jovian planets. Bull. Am. Astron. Soc. 21, 946.

Dowling, T.E., Fischer, A.S., Gierasch, P.J., Harrington, J., LeBeau, R.P., Santori, C.M., 1998. The Explicit Planetary Isentropic-Coordinate (EPIC) atmospheric model. Icarus 132, 221–238. https://doi.org/10.1006/icar.1998.5917.

Fletcher, L.N., 2017. Cycles of activity in the Jovian atmosphere. Geophys. Res. Lett. 44, 4725–4729. https://doi.org/10.1002/2017GL073806.

Fletcher, L.N., Greathouse, T.K., Orton, G.S., Sinclair, J.A., Giles, R.S., Irwin, P.G.J., Encrenaz, T., 2016. Mid-infrared mapping of Jupiter's temperatures, aerosol opacity and chemical distributions with IRTF/TEXES. Icarus 278, 128–161. https://doi.org/10.1016/j.icarus.2016.06.008.

Fletcher, L.N., Orton, G.S., Rogers, J.H., Giles, R.S., Payne, A.V., Irwin, P.G.J., Vedovato, M., 2017. Moist convection and the 2010-2011 revival of Jupiter's South Equatorial Belt. Icarus 286, 94–117. https://doi.org/10.1016/j.icarus.2017.01.001.

Foster, C., Rogers, J., Mizumoto, S., Orton, G., Hansen, C., Momary, T., Casely, A., 2020. A rare methane-bright outbreak in Jupiter's South Temperate domain. In: *14th Europlanet Science Congress 2020*, id. EPSC2020-196.

García-Melendo, E., Sánchez-Lavega, A., Dowling, T.E., 2005. Jupiter's 24° N highest speed jet: vertical structure deduced from nonlinear simulations of a large-amplitude natural disturbance. Icarus 176, 272–282. https://doi.org/10.1016/j.icarus.2005.02.012.

García-Melendo, E., Hueso, R., Sánchez-Lavega, A., Legarreta, J., del Río-Gaztelurrutia, T., Pérez-Hoyos, S., Sanz-Requena, J.F., 2013. Atmospheric dynamics of Saturn's 2010 giant storm. Nat. Geosci. 6, 525–529. https://doi.org/10.1038/ngeo1860.

Gierasch, P.J., Ingersoll, A.P., Banfield, D., Ewald, S.P., Helfenstein, P., Simon-Miller, A., Vasavada, A., Breneman, H.H., Senske, D.A., the Galileo Imaging Team, 2000. Observation of moist convection in Jupiter's atmosphere. Nature 403, 628–630. https://doi.org/10.1038/35001017.

Guillot, T., Stevenson, D.J., Atreya, S.K., Bolton, S.J., Becker, H.N., 2020a. Storms and the depletion of Ammonia in Jupiter: I. microphysics of "Mushballs". J. Geophys. Res. Planets 125, e06403. https://doi.org/10.1029/2020JE006403.

Guillot, T., Li, C., Bolton, S.J., Brown, S.T., Ingersoll, A.P., Janssen, M.A., Levin, S.M., Lunine, J.I., Orton, G.S., Steffes, P.G., Stevenson, D.J., 2020b. Storms and the depletion of Ammonia in Jupiter: II. Explaining the Juno observations. J. Geophys. Res. Planets 125. https://doi.org/10.1029/2020JE006404 article id. e06404.

Hueso, R., Sánchez-Lavega, A., 2001. A three-dimensional model of moist convection for the giant planets: the Jupiter case. Icarus 151, 257–274. https://doi.org/10.1006/icar.2000.6606.

Hueso, R., Sánchez-Lavega, A., Guillot, T., 2002. A model for large-scale convective storms in Jupiter. J. Geophys. Res. Planets 107, 5075. https://doi.org/10.1029/2001JE001839.

Hueso, R., Sánchez-Lavega, A., Iñurrigarro, P., Rojas, J.F., Pérez-Hoyos, S., Mendikoa, I., Gómez-Forrellad, J.M., Go, C., Peach, D., Colas, F., Vedovato, M., 2017. Jupiter cloud morphology and zonal winds from ground-based observations before and

during Juno's first perijove. Geophys. Res. Lett. 44, 4669–4678. https://doi.org/10.1002/2017GL073444.

Hueso, R., Iñurrigarro, P., Sánchez-Lavega, A., Foster, C.R., Rogers, J.H., Orton, G.S., Hansen, C., Eichtaëdt, G., Ordonez-Etxeberria, I., Rojas, J.F., Brueshaber, S.R., Sanz-Requena, J.F., Pérez-Hoyos, S., Wong, M.H., Momary, T., Jónsson, B., Mizumoto, S., Antuñano, A., Pérez-Hoyos, S., Baines, K.H., Dahl, E.K., Go, C., Anguiano-Arteaga, A., 2022. Convective storms in closed cyclones in Jupiter's South Temperate Belt: (I) observations. Icarus 380, 114994. https://doi.org/10.1016/j.icarus.2022.114994.

Ingersoll, A.P., Gierasch, P.J., Banfield, D., Vasavada, A.R., Galileo Imaging Team, 2000. Moist convection as an energy source for the large-scale motions in Jupiter's atmosphere. Nature 403, 630–632. https://doi.org/10.1038/35001021.

Ingersoll, A.P., Dowling, T.E., Gierasch, P.J., Orton, G.S., Read, P.L., Sánchez-Lavega, A., Showman, A.P., Simon-Miller, A.A., Vasavada, A.R., 2004. Atmospheric dynamics. In: Bagenal, F., et al. (Eds.), Jupiter: The Planet, Satellites and Magnetosphere. Cambridge University Press, New York, pp. 105–128.

Iñurrigarro, P., Hueso, R., Legarreta, J., Sánchez-Lavega, A., Eischtädt, G., Rogers, J.H., Orton, G.S., Hansen, C.J., Pérez-Hoyos, S., Rojas, J.F., Gómez-Forrellad, J.M., 2020. Observations and numerical modelling of a convective disturbance in a large-scale cyclone in Jupiter's South Temperate Belt. Icarus 336, 113475. https://doi.org/10.1016/j.icarus.2019.113475.

Legarreta, J., Sánchez-Lavega, A., 2008. Vertical structure of Jupiter's troposphere from nonlinear simulations of long-lived vortices. Icarus 196, 184–201. https://doi.org/10.1016/j.icarus.2008.02.018.

Li, C., Ingersoll, A., Janssen, M., Levin, S., Bolton, S., Adumitroaie, V., Allison, M., Arballo, J., Bellotti, A., Brown, S., Ewald, S., Jewell, L., Misra, S., Orton, G., Oyafuso, F., Steffes, P., Williamson, R., 2017. The distribution of ammonia on Jupiter from a preliminary inversion of Juno microwave radiometer data. Geophys. Res. Lett. 44, 5317–5325. https://doi.org/10.1002/2017GL073159.

Li, C., Ingersoll, A., Bolton, S., Levin, S., Janssen, M., Atreya, S., Lunine, J., Steffes, P., Brown, S., Guillot, T., Allison, M., Arballo, J., Bellotti, A., Adumitroaie, V., Gulkis, S., Hodges, A., Li, L., Misra, S., Orton, G., Oyafuso, F., Santos-Costa, D., Waite, H., Zhang, Z., 2020. The water abundance in Jupiter's equatorial zone. Nat. Astron. 4, 609–616. https://doi.org/10.1038/s41550-020-1009-3.

Lian, Y., Showman, A.P., 2010. Generation of equatorial jets by large-scale latent heating on the giant planets. Icarus 207, 373–392. https://doi.org/10.1016/j.icarus.2009.10.006.

Limaye, S., 1986. Jupiter: new estimates of the mean zonal flow at the cloud level. Icarus 65, 335–352. https://doi.org/10.1016/0019-1035(86)90142-9.

Little, B., Anger, C.D., Ingersoll, A.P., Vasavada, A.R., Senske, D.A., Brenemen, H.H., Borucki, W.J., the Galileo SSI Team, 1999. Galileo images of lightning on Jupiter. Icarus 142, 306–323. https://doi.org/10.1006/icar.1999.6195.

Porco, C.C., West, R.A., McEwen, A., Del Genio, A.D., Ingersoll, A.P., Thomas, P., Squyres, S., Dones, L., Murray, C.D., Johnson, T.V., Burns, J.A., Brahic, A., Neukum, G., Veverka, J., Barbara, J.M., Denk, T., Evans, M., Ferrier, J.J., Geissler, P., Helfenstein, P., Roatsch, T., Throop, H., Tiscareno, M., Vasavada, A.R., 2003. Cassini Imaging of Jupiter's Atmosphere, Satellites, and Rings. Science 299, 1541–1547. https://doi.org/10.1126/science.1079462.

Read, P.L., Kennedy, D., Lewis, N., Scolan, H., Tabataba-Vakili, F., Wang, Y., Wright, S., Young, R., 2020. Baroclinic and barotropic instabilities in planetary atmospheres, energetics, equilibration and adjustment. Non linear processes in Geophysics 27, 147–173. https://doi.org/10.5194/npg-27-147-2020.

Sánchez-Lavega, A., Gómez, J.M., 1996. The South Equatorial Belt of Jupiter, I: Its life cycle. Icarus 121, 1–17 (1996). https://doi.org/10.1006/icar.1996.0067.

Sánchez-Lavega, A., Orton, G.S., Hueso, R., García-Melendo, E., Pérez-Hoyos, S., Simon-Miller, A., Rojas, J.F., Gómez, J.M., Yanamandra-Fisher, P., Fletcher, L., Joels, J., Kemerer, J., Hora, J., Karkoschka, E., de Pater, I., Wong, M.H., Marcus, P.S., Pinilla-Alonso, N., Carvalho, F., Go, C., Parker, D., Salway, M., Valimberti, M., Wesley, A., Pujic, Z., 2008. Depth of a strong jovian jet from a planetary-scale disturbance driven by storms. Nature 451, 437–440. https://doi.org/10.1038/nature06533.

Sánchez-Lavega, A., Rogers, J.H., Orton, G.S., Garcí-a-Melendo, E., Legarreta, J., Colas, F., Dauvergne, J.L., Hueso, R., Rojas, J.F., Pérez-Hoyos, S., Mendikoa, I., Iñurrigarro, P., Gomez-Forrellad, J.M., Momary, T., Hansen, C.J., Eichstaedt, G., Miles, P., Wesley, A., 2017. A planetary-scale disturbance in the most intense Jovian atmospheric jet from Junocam and ground-based observations. Geophys. Res. Lett. 44, 4679–4686. https://doi.org/10.1002/2017GL073421.

Sánchez-Lavega, A., García-Melendo, E., Legarreta, J., Hueso, R., del Río-Gaztelurrutia, T., Sanz-Requena, J.F., Pérez-Hoyos, S., Simon, A.A., Wong, M.H., Soria, M., Gómez-Forrellad, J.M., Barry, T., Delcroix, M., Sayanagi, K.M., Blalock, J. J., Gunnarson, J.L., Dyudina, U., Ewald, S., 2020. A complex storm system in Saturn's north polar atmosphere in 2018. Nat. Astron. 4, 180–187. https://doi.org/10.1038/s41550-019-0914-9.

Sánchez-Lavega, A., Anguiano-Arteaga, A., Iñurrigarro, P., García-Melendo, E., Legarreta, E., Hueso, R., Sanz-Requena, J.F., Pérez-Hoyos, S., Mendikoa, I., Rojas, J.F., Andres-Carcasona, M., Part-Garsull, A., Ordoñez-Etxeberria, I., Rogers, J. H., Foster, C., Mizumoto, S., Casely, A., Hansen, C.J., Orton, G.S., Momary, T., Eischtadt, G., 2021. Jupiter's Great Red Spot: strong interactions with incoming anticyclones in 2019. J. Geophys. Res. Planets 126. https://doi.org/10.1029/2020JE006686 e2020JE006686.

Sankar, R., Palotai, C., 2022. A new convective parameterization applied to Jupiter: implications for water abundance near the 24°N region. Icarus 380, 114973. https://doi.org/10.1016/j.icarus.2022.114973.

Smith, B.A., Soderblom, L.A., Johnson, T.V., Ingersoll, A.P., Collins, S.A., Shoemaker, E. M., Hunt, G.E., Masursky, H., Carr, M.H., Davies, M.E., Cook II, A.F., Boyce, J., Danielson, G.E., Owen, T., Sagan, C., Beebe, R.F., Veverka, J., Strom, R.G., Mccauley, J.F., Morrison, D., Briggs, G.A., Suomi, V.E., 1979a. The Jupiter system through the eyes of Voyager 1. Science 204, 951–957. https://doi.org/10.1126/science.204.4396.951.

Smith, B.A., Soderblom, L.A., Beebe, R., Boyce, J., Briggs, G., Carr, M., Collins, S.A., Cook II, A.F., Danielson, G.E., Davies, M.E., Hunt, G.E., Ingersoll, A., Johnson, T.V., Masursky, H., Mccauley, J., Morrison, D., Owen, T., Sagan, C., Shoemaker, E.M., Strom, R., Suomi, V.E., Veverka, J., 1979b. The Galilean satellites and Jupiter: Voyager 2 imaging science results. Science 206, 927–950. https://doi.org/10.1126/science.206.4421.927.

Stoker, C.R., 1986. Moist convection: a mechanism for producing the vertical structure of the Jovian equatorial plumes. Icarus 67, 106–125. https://doi.org/10.1016/0019-1035(86)90179-X.

Stratman, P.W., Showman, A.P., Dowling, T.E., Sromovsky, L.A., 2001. EPIC simulations of bright companions to Neptune's Great Dark Spots. Icarus 151, 275–285. https://doi.org/10.1006/icar.2001.6603.

Sugiyama, K., Nakajima, K., Odaka, M., Kuramoto, K., Hayashi, Y.-Y., 2014. Numerical simulations of Jupiter's moist convection layer: structure and dynamics in statistically steady states. Icarus 229, 71–91. https://doi.org/10.1016/j.icarus.2013.10.016.

Thomson, S.I., McIntyre, M.E., 2016. Jupiter's unearthly jets: a new turbulent model exhibiting statistical steadiness without large-scale dissipation. J. Atmos. Sci. 73 (3) https://doi.org/10.1175/JAS-D-14-0370.1.

Vasavada, A., Showman, A.P., 2005. Jovian atmospheric dynamics: an update after Galileo and Cassini. Rep. Prog. Phys. 68, 1935–1996. https://doi.org/10.1088/0034-4885/68/8/R06.

Young, R.M.B., Read, P.L., 2017. Forward and inverse kinetic energy cascades in Jupiter's turbulent weather layer. Nat. Phys. 13, 1135–1140. https://doi.org/10.1038/nphys4227.